Journal of Geomorphology, Vol. 1/1 (2022), 79–102
Published Early Access August 19, 2022, published online December 2022

Automated landform classification and mapping using a combined textural-morphometric approach: the Congo basin and surroundings

Gaëlle Viennois[1,*], François Bétard[2], Vincent Freycon[3,4], Nicolas Barbier[1,5], Pierre Couteron[1,5]

[1] AMAP, IRD, CIRAD, CNRS, INRA, Univ Montpellier, Montpellier, France
[2] Université Paris Cité, UMR 8586 PRODIG, Paris, France
[3] CIRAD, UPR Forêts et Sociétés, F-34398 Montpellier, France
[4] Forêts et Sociétés, Univ Montpellier, CIRAD, Montpellier, France
[5] International Joint Laboratory DYCOFAC, IRD-UYI-IRGM, Yaound'e P.O Box 1857, Cameroon
* Corresponding author: gaelle.viennois@cirad.fr

With 6 figures and 4 tables

Abstract: An automatic method of landform mapping applicable to large continental areas is presented, based on 30-meter SRTM (Shuttle Radar Topography Mission) data and combining texture analysis using Fourier 2D periodograms (FOTO method) with a set of morphometric variables. This integrated strategy was applied to the whole Congo Basin and adjacent regions in Central Africa, where landscapes and landforms mapping remains heterogeneous and partial with existing expert maps differing in aims and scales. Through the FOTO method, a principal component analysis (PCA) on obtained Fourier r-spectra yielded six textural features, which were further combined with seven morphometric criteria into a global PCA. A k-means classification from these output results provided an automatic mapping of 12 landform classes (at a final resolution of 900 m) which were successfully interpreted in terms of geomorphological meaning together with some hydrological and soil attributes. Finally, comparison of our landform map with existing, independent geomorphological sheets revealed a good spatial congruence. Overall, our method proved effective to depict landform assemblages at regional or continental scales based on complementary textural information and morphometric parameters. As such, it could serve as a sound basis for further predicting and mapping soil units at the landscape scale, given the close soil-landform imbrications and interactions at the *catena* level. It could serve as well as a predictive variable for biodiversity measures and biomass estimates, especially in the humid tropics where environmental data are lacking whilst ecological modelling is urgently needed to support land planning and forest management.

Keywords: SRTM; geomorphological mapping; texture; morphometry; Congo basin

1 Introduction

Geomorphological maps have potential applications in many fields including geomorphology, ecology, soil science, hydrology, agriculture and civil engineering (Drăguţ & Eisank 2012), each of which has historically been involved with the classification and mapping of landforms as an essential component of land systems and landscapes. For instance, in landscape ecology studies, geomorphological heterogeneity is considered as an important driver of ecological complexity and biodiversity patterns at alpha, beta and gamma levels (Burnett et al. 1998, Nichols et al. 1998, Tukiainen et al. 2019). In tropical rainforests like Amazonia, geomorphological diversity (or geomorphodiversity: Panizza 2009) proved to be a key factor in accounting for differences in floristic richness, forest structure and carbon stocks together with edaphic variations (Figueiredo et al. 2014, Guitet et al. 2015a, Guitet et al. 2015b, Guitet et al. 2016). Links between landforms and soil systems are also well recognized (Birkeland 1999, Gerrard 1992, Schaetzl & Anderson 2005). Geomorphological mapping, which was implemented by many scientists from the French School of pedology, has illustrated its efficiency for soil mapping in tropical regions, with direct applications for land evaluation and agronomic

DOI: 10.1127/jgeomorphology/2022/0752

Gebrüder Borntraeger Science Publishers, Stuttgart, www.borntraeger-cramer.de

purposes ("morphopedological mapping": Bétard & Bourgeon 2009).

Historically, geomorphological maps were produced manually by visual interpretation of aerial photographs or topographic maps at various resolutions and scales, with aims and methods specific to each country and proper to each author. Consequently, it is impossible to compare them without a continuous and homogenous mapping basis. It also hinders their use for interpreting broad scale biogeographic patterns or for designing consistent land resource maps. Yet, the availability and accessibility of remotely sensed Digital Elevation Models (DEMs), and the improvement of processing techniques have made possible to develop geomorphometry, with the fundamental operation of extracting parameters and objects from DEMs (Pike et al. 2009). Generation of high-resolution DEMs has recently led to a paradigm shift in geomorphometry (Drăguț et al. 2011, Evans 2012), with growing interest to classify and map minor landforms, either natural or anthropogenic, at very fine scales (e.g., landform extraction and mapping from LiDAR DEMs (De Matos-Machado et al. 2019, Ortuño et al. 2017). Paradoxically, available global Digital Surface Models (DSM), with coarser resolution, such as those of the Shuttle Radar Topography Mission (SRTM) exist for a longer time than high-resolution DEMs and have proved efficient in the field of ecological modelling (Amatulli et al. 2018, Moudrý et al. 2018) but are still underused from this perspective of landform mapping. Although DSMs provide top of vegetation elevation data and are not Digital Terrain Model (DTM) i.e. elevations at ground level, their use for producing broad-scale geomorphological maps is worth considering (e.g., Iwahashi & Pike 2007, Bugnicourt et al. 2018).

Methodological developments of automated or semi-automated processing of DEMs are more than ever required to elaborate robust and consistent landform maps at broad scales (Drăguț & Eisank 2012, Iwahashi & Pike 2007), given the huge surfaces to cover and the necessity of iterative processes to implement and assess the classification of continuous topography. In this paper, we use the term *landforms* to define areal geomorphic objects as detected on DEMs (with x/y coordinates) and having a third dimension in z (Evans 2012). Automated or semi-automated detection of *geometric signatures* on DEMs (Pike 1988) may allow us to further identify *landform types. Geometric signatures* are defined by Iwahashi and Pike (2007) as "a set of measures that describes topographic form to distinguish geomorphologically disparate landscapes", whereas *landform types* are defined by MacMillan et al. (2000) as "assemblages of repeating patterns of landform elements with characteristic patterns and scales of repetition". In a recent study, Bugnicourt et al. (2018) combined the Fourier-based textural ordination (FOTO) method (Couteron 2002) with geometric signatures of a set of morphometric variables to characterize 16 landform types in a humid tropical region of 220,000 km^2 (French Guiana and Amapa, Brazil). To our knowledge, this method has not been tested in other contexts. The generic principles on which the method relies makes it attractive to adapt and test with respect to other situations, possibly over broader areas in the humid tropics for which geomorphic information is lacking.

This is the case of Central Africa, where the Congo Basin straddles six countries and includes the world's second largest continuous area of tropical forests behind Amazonia. This region is experiencing a context of growing demand for resource assessment and land-use planning, with major environmental issues such as destruction of peatland forests and associated huge soil carbon stocks (Dargie et al. 2017). Consequently, this region needs landform classification and mapping at a regional scale, but available geomorphological maps are old and expert-based products with aims, scales and methods specific to each individual study, that prevents any map generalization.

The main goal of this paper is to promote the valid and robust use of a combined textural-morphometric approach dedicated to landform classification and mapping at very broad scales, with application to the whole Congo Basin and surroundings in Central Africa. The proposed method is an adapted version of the automatic method developed in reference to a smaller portion of tropical South America by Bugnicourt et al. (2018). Comparisons to existing maps based on expert knowledge are integrated parts of the method without constituting a validation process as such. The objective is not to reproduce these expert maps but rather to produce a synthetic, homogeneous map able to render the most interpretable, fairly consensual geomorphic elements of the experts' works for subcontinental scale landform depiction. By comparing, we aim at assessing to what extent our map may sustain similar interpretation as experts, while addressing the very large, unmapped areas, in fact most of Central Africa. We hypothesized that (1) textural and morphometric descriptors are complementary and their combined use allows sensible and homogeneous, automated landform-type mapping over very large areas; (2) the general map of landform classes obtained is in its broad line consistent with the expert-based maps that had specific aims and methods, and is therefore relevant to provide a wall-to-wall geomorphological mapping over Central Africa.

In this paper, we first describe the processing flow from the SRTM, that features the textural analysis associated with the calculation of morphometric parameters followed by a general PCA as to arrive at a final classification of 12 landform classes. Secondly, we interpret

the 12 landform classes and compare them with existing expert maps that concerns some parts of the studied region. Finally, we check for possible biases from forest-savanna mosaics due to the use of the SRTM (i.e. a DSM), before discussing the overall results.

2 Materials and methods

2.1 Study area

Our study area encompasses the Congo Basin and adjacent regions, including the following six countries: Gabon, Cameroon, Central Africa Republic, Republic of Congo, Democratic Republic of Congo and Equatorial Guinea, with a total surface of *ca* 2,696,500 km² (Fig. 1A). The area extends from the Atlantic Ocean to the West (Gulf of Guinea) to the western shoulder of the Albertine Rift Valley to the East, and spans the equator between 7° N and 5° S. It is centered on the Congo Basin which harbors the world's second largest continuous area of rainforest behind Amazonia (Verbeeck et al. 2011). This includes a variety of forest types pigeonholed into broad bioclimatic (wet, moist, dry forests) or functional forest classes (evergreen, deciduous) as reviewed by Fayolle et al. (2014), and several studies have underlined the link between certain of those types and geological substrates (Fayolle et al. 2012, Réjou-Méchain et al. 2008). The study area is bisected by the equator, and therefore displays little seasonal variation within 1° North or South of the equator. Seasonality increases with distance from the equator, with two rainy seasons including very high rainfall alternating with two drier seasons. The climate remains warm and humid with mean temperatures ranging from 22 °C to 30 °C and average rainfall between 1200 and 2600 mm per year (Leroux 2001).

Topographically, the center of the Congo Basin forms a huge depression with little relief variation – named "Cuvette Centrale" or Central Basin – drained by the Congo River and its tributaries. These low wetlands are covered by extensive peat soils beneath swamp forest vegetation, recently considered as the largest peatland complex in the tropics (Dargie et al. 2017). At the periphery of the Congo Basin, the altitudes of this flat-lying topography progressively increase toward surrounding plains and plateaus (e.g., Batéké, Carnot-Gadzi and Mouka-Ouadda plateaus) through successive stepped topographic levels, from 200 m a.s.l in the Central Basin to 1,000 m a.s.l. on its highest margins. Toward the Atlantic Ocean, a collection of mountainous massifs and chains forms a marginal bulge (Mayombé, Crystal and Chaillu mountains) above a narrow coastal strip (Petit 1990). To the North, these mountains extend into the Cameroon range where the Mount Cameroon constitutes the most prominent peak culminating at 4,040 m a.s.l.

From a geological viewpoint (Fig. 1B), the Congo Basin is a broad downwarp centered on the Congo craton, with thick accumulations of near-horizontal sediments of Meso-Cenozoic age, mainly deposited in continental (lacustrine, fluvial) conditions with few marine incursions (Giresse 2005). This extensive sedimentary cover, dominated by sandy deposits and sandstone lithologies (e.g., *Sables Ocres* and *Grès Polymorphes* Series of Cenozoic age), appears in sharp contrast with the varied basement rocks outcropping at the periphery of the basin. Remnants of the Archean nuclei, also known as the "West Central Africa" craton (Milesi et al. 2006), are well represented to the West of the study area (southern Cameroon, Equatorial Guinea, Gabon and Congo): they are composed of various granite-gneiss complexes and greenstone belts. These Archean remnants are juxtaposed with folded Proterozoic belts ("Pan-African" belts) characterized by the presence of wide NE-SW-trending shear zones. All the rocks in these belts are metasedimentary and volcano-sedimentary (various kyanite schists and gneisses, migmatites, amphibolites and quartzites) together with metaplutonic rocks of amphibolite to granulite facies. Finally, the Cameroon Line located to the Northwest defines a 1000-km-long line of volcano-capped swells of basaltic composition, both lying on land and in the Gulf of Guinea, and usually interpreted as related to an underlying mantle plume (Burke 2001). Such a complex geological setting with varied lithologies and tectonic styles is prone to high geomorphological heterogeneity, as expected on our landform mapping.

2.2 Data

All the analyses necessary to produce the landform map of Congo Basin were carried out from Shuttle Radar Topography Mission (SRTM) dataset at 1 Arc-Second Global (30 m), acquired by NASA in February 2000 and made available with the considered resolution in 2013. The SRTM data were collected by a single-pass interferometric synthetic aperture radar system (Band C) (Farr et al. 2007). These data have the specificity to represent ground surface topography as well as features above the ground including man-made structures and vegetation. For constant vegetation height as is the case over large forests, SRTM data can be approximated as a DEM with a vertical accuracy of *ca* 10 m (Bourgine & Baghdadi 2005). Although forests are by far the most extended vegetation form in the study area, there are also landscapes covered by open vegetation (savannas, grasslands, etc.) or more critically by forest-savanna-mosaics. A post-hoc assessment of possible problems was made by evaluating the extent of such mosaics in the various landform

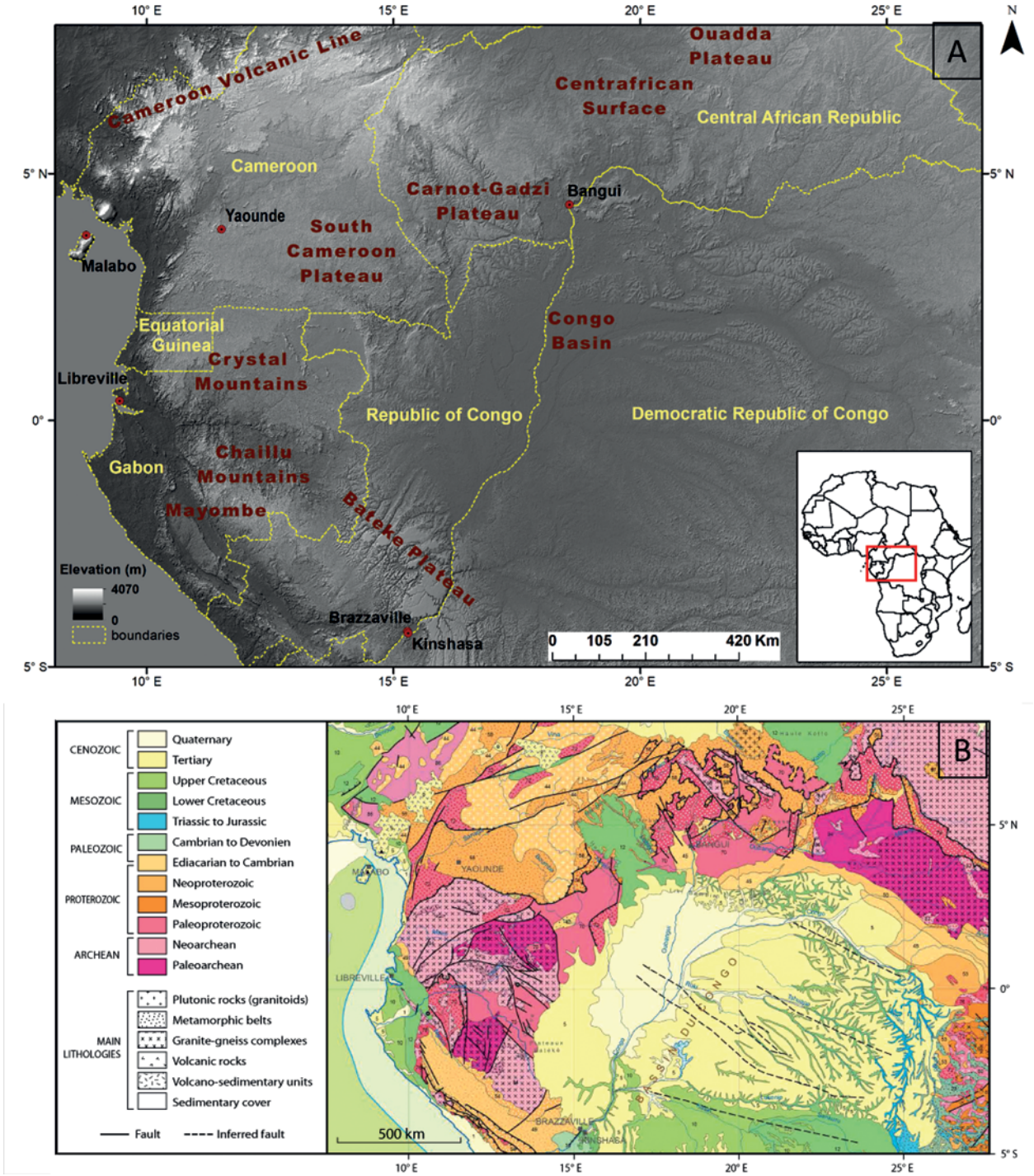

Fig. 1. Location and geological setting of the study area. **A:** Topography of the study area with the main physiographic units adapted from Petit (1990); Area covered = 2,696,502 km². **B:** Simplified geological map of the study area adapted from Thiéblemont (2016).

Table 1. Characteristics of existing maps. * Percentage of the area of the map made by the expert in relation to the total area of our study area

Area	Type	Author	Scale	Date	% Cover Map*
Southern Cameroon	Soil map	Vallerie (1995)	1 : 500 000	1995	2
Gabon	Soil map	Martin et al. (1981)	1 : 2 000 000	1981	10
Central Africa	Morphology map	Petit (1990)	1 : 14 000 000	1990	64
Central African Republic	Geomorphological map	Boulvert (1996)	1 : 1 000 000	1996	3
Cuvette Centrale wetlands	Peatland probability map	Dargie et al. (2017)	1 : 9 000 000	2017	36
Africa	Topography	Iwahashi & Pike (2007)	1 : 100 000 000	2007	100

classes we defined and mapped (see below). For the selected study area, we downloaded 239 tiles of SRTM Version 3.0 Global 1 in geographic projection WGS84 on http://dwtkns.com/srtm30m/ (access date: 01/02/2020) which we then assembled into a final single image.

In order to benchmark the interpretability of our landform map, we used different existing maps drawn by previous authors from expert-based work. These ancient maps, that stemmed from diverse objectives, cover all or parts of some of the Congo Basin countries, and have therefore different scales and various thematic classifications (Table 1). They follow methods and aims specific to each region or country making them difficult to harmonize or compare. But such maps are complementary in terms of geographical coverage and from a scalar viewpoint.

At a fine scale, the map produced by Vallerie (1995) covers the south of Cameroon. At broader scale, the map produced by Martin et al. (1981) covers the entire Gabon. These two maps aimed to represent soil-landform categories (or "morphopedological units"). At medium scale, the map produced by Boulvert in 1996 covers all the Central African Republic and represents geomorphological features. This map was provided by the map library of IRD (http://sphaera.cartographie.ird.fr/) in georeferenced image format. Petit (1990) produced a large-scale morphological map that covers all Central Africa. These four maps were based on photo-interpretation and/or by sketching from expert knowledge. Two recent maps were also used for comparison with our final product: the Peatland probability map covering the Cuvette Centrale Wetlands by Dargie et al. (2017) from an array of remote sensing data (http://www.afritron.org/en/peatland) and the worldwide topography map made by Iwahashi and Pike (2007) from digital processing of SRTM data (http://gisstar.gsi.go.jp/terrain/front_page.htm).

2.3 Methods

To address the mapping of landforms at the very broad scale of the Congo Basin, we adapted the automatic method developed in tropical South America by Bugnicourt et al. (2018). Briefly, we analyzed the textural information (Couteron et al. 2006) of SRTM using a multiscale approach as to assess areal geometric signatures. Then we combined main textural features and a set of common morphometric criteria also derived from SRTM data in order to provide complementary information on the relief dimension in z (Evans 2012). Figure 2 shows the workflow that summarizes the different steps leading to the final landform map.

2.3.1 Textural analysis

The textural analysis of SRTM allowed us to extract *geometric signatures*. We used Fourier-based textural ordination (FOTO) method (Couteron 2002) to analyse the texture. This method has extensively been used for vegetation mapping (Couteron 2002, Proisy et al. 2007), land-use/cover studies (Couteron et al. 2006), and more recently for regional-scale extraction of geomorphic signatures from SRTM data (Bugnicourt et al. 2018). The detailed description of the method is provided in Couteron (2002), and we here just recall the main outlines regarding its present application. FOTO subdivides the SRTM image in square windows and analyses spatial variations of the SRTM grey levels through the Fourier two-dimensional periodogram. The size of the window expresses a trade-off between homogeneity of the landforms depicted through textural features and sufficient extent to characterize large landforms. Considering the wide size range of landforms usually displayed, we used here two window sizes (29 and 299 SRTM pixels, corresponding to two different scales of *ca* 1 km and *ca* 10 km) centered on the pixels of the same overall grid. Bugnicourt et al. (2018) found that 9 km windows were large enough to render broad landforms (e.g. mountains and main ridges), while texture gradients using a substantially smaller size (6 km) did not provide important information regarding intermediate-sized landforms. To complement the 10 km-window analysis we therefore selected a second size being one order of magnitude

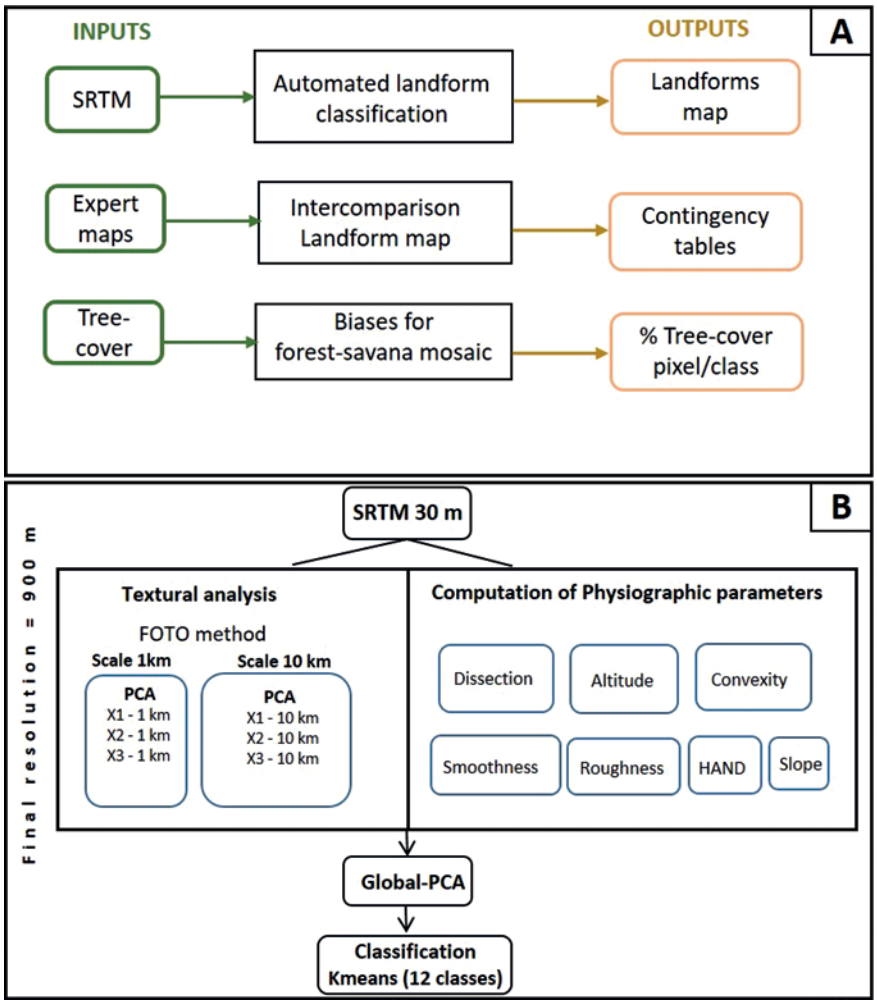

Fig. 2. Workflow of the main steps of the methodology **(A)** and processing steps towards automated landform classification **(B)**.

below (1 km) as to improve accuracy in depicting small landforms. Moreover, we also used sliding windows that overlap to increase the output spatial resolution of textural features up to 900 m for both window sizes. In each window, the 2D Discrete Fourier Transform is applied on SRTM values leading to the calculation of the 2D periodogram. FOTO then summarizes the 2D periodograms by calculating azimuthally averaged r-spectra that are assembled in a matrix in which windows are rows and spatial frequencies are columns. R-spectra directly express the broken-down of image variance for the harmonic spatial frequencies of Fourier analysis. A standardized principal component analysis (PCA; Manly & Alberto 2016) is performed on this matrix to compare r-spectra and thereby texture over a very large number of windows. In so doing, PCA orders windows along texture gradients and very often the first axis opposes the coarsest textures to fine textures while the second axis often characterizes intermediate textures that are frequently opposed to heterogeneous windows. At the end, we kept the first three axes of the two scales of analysis (1 km and 10 km windows) as new synthetic variables that summarize textural variation. We combined the two triplets of PCA axes into a general PCA of texture and use the resulting scores of windows as final textural features for use in subsequent analyses. Those scores were also submitted to k-means clustering into 12 textural classes.

2.3.2 Computation of morphometric parameters and final classification

In addition to textural features, we selected and used seven morphometric criteria as to render elevation magnitude and topographic variation in windows. Such criteria, also derived from SRTM data (see the complete list, calculation methods and related references in Table 2) and display strong complementarity with textural features

Table 2. Morphometric parameters retained in the methodology.

Criteria	Factor	Computation	Reference
Dissection	Relative elevation range	(max elev. - min elev.) / mean elev.	Bugnicourt et al. (2018)
Elevation	Mean elevation	Mean value at 900 m resolution	
Convexity	Mean convexity	Saga: Terrain surface convexity	
Smoothness	Area with gentle slope	Number of pixels with slope <15%	Guitet et al. (2013)
Roughness	Area with steep slope	Number of pixels with slope >30%	Guitet et al. (2013)
Slope	Mean slope	Mean value at 900 m resolution	
HAND	Height Above Nearest Drainage	Mean value at 900 m resolution	Rennó et al. (2008) and Guitet et al. (2013)

(Bugnicourt et al. 2018). Under the ESRI ArcGIS 10.7.1 ® software, we calculated the terrain slope and the Height Above the Nearest Drainage (HAND) index, this last being a proxy for estimating local soil water condition (Rennó et al. 2008). Slope convexity was calculated using SAGA 2.3.2® software, while the other indices (Dissection, Altitude, Smoothness and Roughness) were computed by using the free statistical software package R 3.6.3. All the seven criteria were computed at a spatial resolution of 900 m. Finally, we applied a "Global PCA" on the seven morphometric criteria and the six texture variables from the FOTO analysis. We pursued by a k-means classification with 12 output classes.

2.3.3 Map inter-comparison

We referred to the aforementioned set of maps based on expert knowledge, to make comparisons with the results of our automated mapping approach. However, this comparison should not be considered as a validation process. First, the reference maps entail subjectivity. Second, though integrating geomorphological reasoning, the authors of the maps pursued varied objectives in terms of areas covered and topics, which are distinct from ours. Yet, all the maps we used for comparison did integrate some geomorphological reasoning, and our aim while comparing is to assess to what extent our mapping is able to retrieve broad common geomorphic patterns whose mapping may be useful for a variety of topics related to tropical landforms and landscapes.

In order to make the existing maps comparable with our landform map, we had to do some reinterpretation work. First, some maps covering limited areas were too detailed such as the soil map of South Cameroon of Vallerie (1995) with 22 map units represented. We took opportunity of the explicit reference of the soil units to geomorphology ("morphopedological approach": Bétard & Bourgeon 2009, Birkeland 1999, Gerrard 1992) to reduce this number of entities to 11 and renamed them in terms of landform units. Second, the units of the geomorphological map of the Central African Republic (Boulvert 1996) represent a mixture of geological and geomorphological names that are not comparable as such. So it was necessary to interpret some geological entities in terms of geomorphological units in agreement with the legend of (Boulvert 1996). For instance, the rocks of the Precambrian complex (crystalline facies, crystallophyllian and basic rocks) are geologically fairly homogeneous and are, from a geomorphological viewpoint, linked to more or less degraded elements of the "*surface centrafricaine*" (Burke & Gunnell 2008), while carbonate facies correspond to a low-relief karstified surface belonging to the Ouganbian piedmont. We georeferenced and digitized parts of the South Cameroon and Central African Republic maps (footprints corresponding to our map) and the entire maps of Gabon and Central Africa under ESRI ArcGIS 10.7.1 ® software. We finally cross-referenced them with our landform map of Congo Basin and produced contingency tables from cross-classification. To ease the analysis of the contingency tables, we computed corrected frequencies (Equation 1) that basically are ratios of observed to expected areas in the cells of the contingency tables. Namely,

$$fij = n++ * \frac{nij}{ni +* n+j} \qquad \text{Eq. 1}$$

where nij is the area classified in cell i, j, ni_+ is the total area relating to class i and vice-versa for n_+j. n_{++} is the total studied area. We then considered fij-1, so that values greater than zero reflect a correspondence between two categories of the compared maps and vice-versa for negative values. We finally used a Chi-square test per cell (Sokal & Rohlf 1981) on the contingency tables to highlight cells with significant departures of fij above 1 and corresponding positive associations between the classes of the two maps under comparison.

2.3.4 Checking for possible biases from forest-savanna mosaics

As post-hoc assessment we cross-referenced our final map of 12 classes with Global tree cover (treecover2010,

https://glad.umd.edu/dataset/global-2010-tree-cover-30-m, access date: 01/03/2021) which are per pixel (0.09 ha) estimates of percent maximum (peak of growing season) tree canopy cover derived from annual growing season composite Landsat 7 ETM+ data. We sampled 300,000 points and produced histograms to study the distribution of tree canopy cover in each of our geomorphological classes. We thereby looked for the classes in which savanna–forest mosaics significantly occur, as to investigate to what extent variation in vegetation height (generally less than 40 m) may bias the geomorphic features that were most distinctive of a class, and may thereby induce a risk of confusion with other classes.

3 Results and interpretation

3.1 Textural gradients and classes

Both window sizes yielded analogous textural gradients through the PCA axes ordinating r-spectra. The first axes expressed a gradient between coarse vs. fine texture, and a second axis reflected an opposition between rather homogeneous patterns of intermediate texture and heterogeneous patterns integrating both fine and coarse texture (Appendix E). In spite of a large contrast in window size, the two systems of axes proved thus inter-correlated, though the larger window size allows integrating larger patterns while the smaller size enabled finer distinctions in the fine-grained domain. The relevance of synthetizing the two systems of axes through a general PCA was thus verified and the resulting scores provided a safe basis for defining textural classes through k-means clustering.

In Fig. 3, we present some arbitrarily selected windows which typify the 12 textural classes as to illustrate the link between visual perception and shapes of spectra. In log-log coordinates, we expect self-similar patterns (i.e. fractal-like), devoid of any dominant periodicity to display fairly linear spectra indicating a rapid concentration in spectral power (i.e. variance fractions) for large wavelengths (Bugnicourt et al. 2018, Couteron et al. 2006) as for instance with classes 6 and 11. Conversely, departures from a straight line point towards spatial periodicity through characteristic wavelengths. For instance, spectra displayed for classes 8, 3, 10, 2 and 12, show a levelling-off when approaching large spatial wavelengths (e.g. a change in slope at *ca* 1 km for class 10). This means that wavelengths just below the cutting point or around the spike (e.g. class 1) concentrate more variance than expected for a self-similar patterns and thus points towards characteristic features of strong periodicity. This is mainly observed when approaching large wavelengths and therefore clearer from the larger window size (set B), though already perceptible with the smaller size (A).

3.2 Integrating the morphometric parameters

Figure 4 shows the results of the Global PCA (G-PCA) integrating the six synthetic textural features along with the seven physiographic criteria (for detail of each criteria, see the Table 3). The eigenvalues of the three first axes (Fig. 4A) reached 27%, 23% and 18% respectively, accounting all together for 68% of variance explained. The correlation circle (Fig. 4B) shows that axis 1 is mainly composed by Dissection, Convexity and Roughness on the negative side opposed to Smoothness and the first axis of FOTO at 10 km scale (fine textures) on the positive side. The second axis mainly relates to textural features (only elevation is notably correlated) and mainly opposed the second and third axes of FOTO for the two scales 1 and 10 km. As a result, physiographic criteria are mainly correlated with axis 1 while textural features are rather correlated with axis 2, thus showing their complementarity.

When we projected a sampling of the 12 k-means classes along the two first axes of G-PCA (Fig. 4C), we noted that axis 1 opposed the classes “low wet plains” and “high wet plains” (classes 1 and 5 respectively, right side) to the classes “high mountain ranges” and “low-medium mountain ranges” (classes 11 and 12 respectively, left side). Classes 1 and 5 have extremely flat reliefs (mean slope of 3.65%, Table 3) and show high wetness (i.e., mean HAND = 13.4 m, Table 3). Classes 11 and 12 are characterized by the highest elevation (mean of 737 m a.s.l.; Table 3) and steep slopes (mean of 29.5%, Table 3). Roughness, Convexity and Dissection are there the highest. Moreover, in terms of texture, classes 11 and 12 show a coarser grain and spectra suggesting self-similarity while classes 1 and 5 have spectra marked by small spatial wavelengths (see also Fig. 3). Axis 2 separates the “Tablelands” represented by the classes 6 and 4 with low roughness values (bottom, mean elevation of 588 m a.s.l., Table 3) from the “Foothills” represented by Class 2 (top). Foothills are characterized by moderate slope gradients (16.07%, Table 3), intermediate elevations (mean of 389 m a.s.l.) and a moderate Dissection (0.21, Table 3). Their texture is characterized by the relative importance of patterns of intermediate wavelengths (1–5 km) determining humped-shaped spectra (Fig. 3). On the contrary, the high tablelands suggest self-similarity (Fig. 3) and notably associate coarse and fine textures, while displaying high Smoothness (mean of 871.7, Table 3) and low Dissection (mean of 0.07 m, Table 3). The remaining classes located around the origin of the two axes show intermediate characteristics (class 7 and

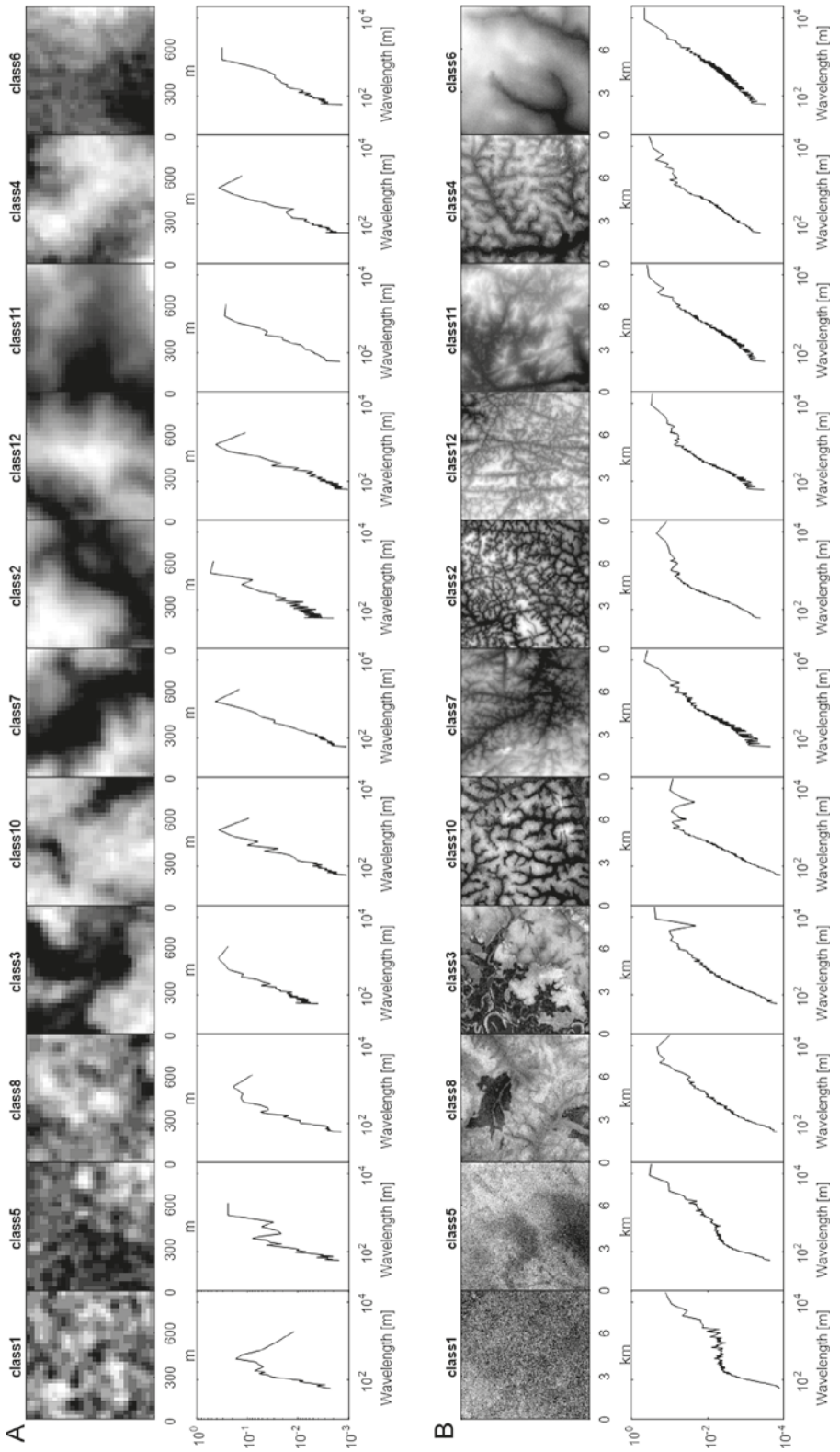

Fig. 3. Samples of typical windows with associated Fourier r-spectra for illustration of the landform classes at two scales of textural analysis: 1 km **(A)** and 10 km **(B)** for the same region. For both sets, the spectra expressed shares of image gray-level variance (*Y*-axis) for spatial wavelengths (abscissa, in meters). For both window sizes **(A)** and **(B)**, windows are ranked from fine-grained to coarse-grained patterns. Patterns characterized by a strong relative contribution of intermediate textures are placed in the middle of the set.

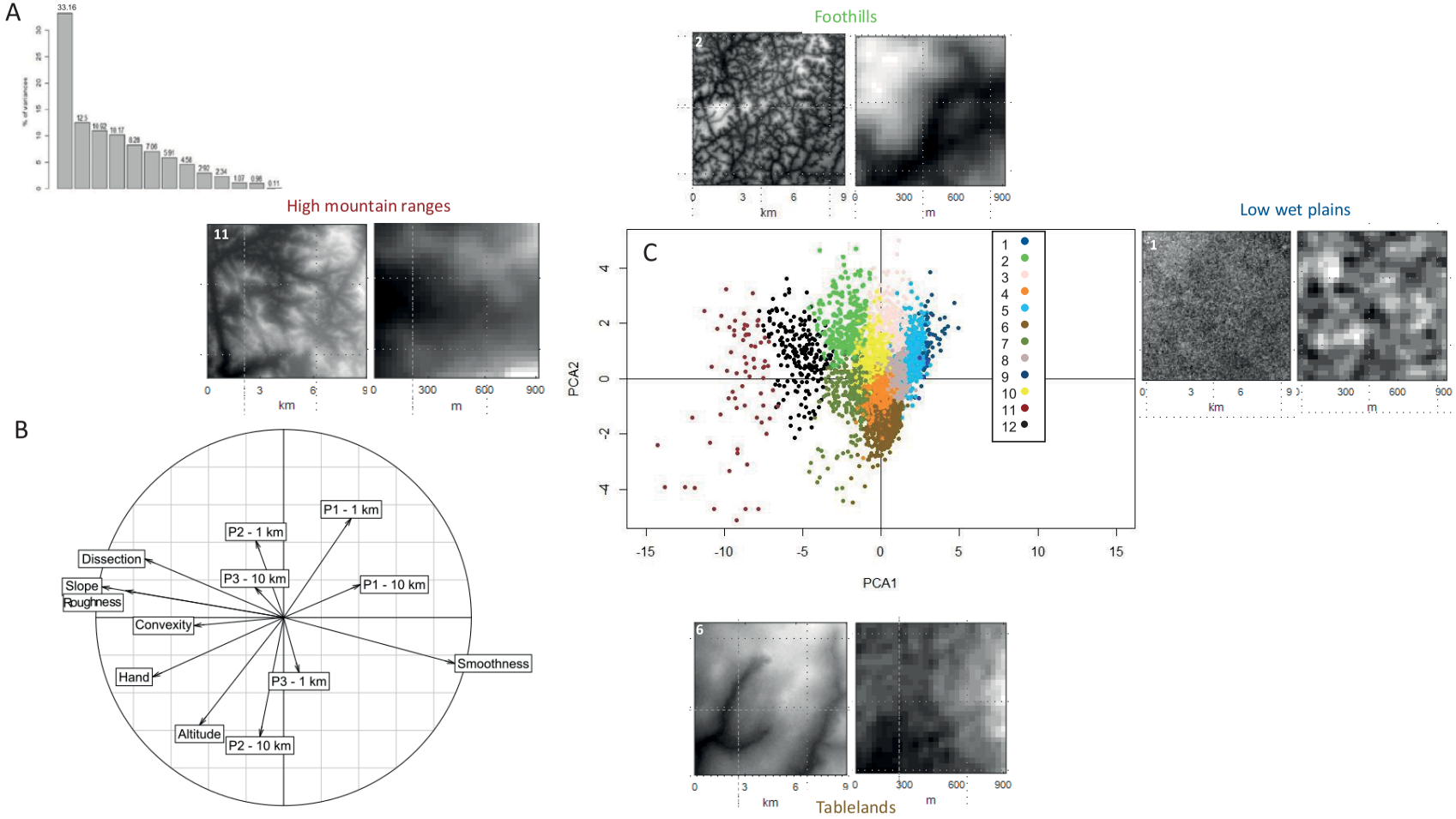

Fig. 4. Results of the G-PCA (integrating textural and morphometric criteria): **(A)** eigenvalues and **(B)** correlation circle of G-PCA along the first two axes with projection of variables used. Projection of 12 k-means classes along the two first axes **(C)**. SRTM windows of 10 km and 1 km represent the four characteristics classes (11, 2, 1 and 6) along the two axes.

Table 3. Morphometric characteristics of the 12 landform classes. We used mean to describe the classes in the text. We used standard deviation to check that the classes were sufficiently homogeneous. Class 11 (high mountain ranges) of our map does not appear within the area covered by Dargie's map; SD: Standard Deviation; * = significant p-value for positive corrected frequencies of Chi-square by cell test

Class	Landform unit	Dissection (m)		Convexity		Elevation (m)		HAND (m)		Slope (%)		Smoothness		Roughness	
		Mean	SD	Mean	SD	Mean	SD	Mean	SD	Mean	SD	Mean	SD	Mean	SD
1	Low wet plains	0.0	0.0	40.2	5.4	327.2	40.8	9.2	15.6	3.1	0.7	898.1	11.1	0.1	1.4
2	Foothills	0.2	0.1	47.0	2.0	389.7	197.5	91.2	66.9	16.1	2.8	465.0	110.4	79.8	57.5
3	Coastal and interior plains (coastal dominant)	0.1	0.1	43.6	2.9	311.0	177.5	27.8	26.9	7.3	2.0	824.2	67.5	1.9	5.4
4	Dissected tablelands	0.1	0.0	43.7	1.6	569.9	148.5	66.3	43.3	8.0	1.8	809.4	67.1	2.9	6.4
5	High wet plains	0.0	0.0	41.5	3.7	349.2	98.5	17.6	28.6	4.1	1.2	890.8	20.0	0.2	2.0
6	Tablelands	0.1	0.0	42.2	1.9	607.0	166.7	92.4	70.0	5.9	1.7	871.7	41.2	1.0	4.6
7	High hills and crests	0.2	0.1	45.3	1.8	592.9	249.2	159.5	120.2	13.9	2.5	564.9	104.7	55.6	45.5
8	Coastal and interior plains (interior dominant)	0.1	0.0	42.7	2.4	399.3	123.7	33.3	28.2	5.8	1.5	866.7	38.0	0.7	3.3
9	Water	0.0	0.0	0.3	3.0	7.9	48.8	0.1	0.9	0.0	0.3	899.8	1.8	0.0	0.3
10	Low hills and plateaus	0.1	0.0	45.1	1.5	507.3	119.6	56.7	36.2	10.1	2.1	718.0	94.2	8.8	12.8
11	High mountain ranges	0.3	0.2	46.6	2.1	933.2	482.9	563.1	338.9	35.1	7.7	125.1	83.9	509.7	150.0
12	Low-medium mountain ranges	0.3	0.1	47.0	2.2	540.4	273.2	218.6	143.4	23.9	3.6	272.2	91.6	270.9	93.7

10). The complex of "Coastal and interior plains" (coastal dominant: class 3; interior dominant: class 8) is characterized by an intermediate hand index (about 30.55m) and a fairly high smoothness index (about 845.5 m). These two classes (3 and 8) are very similar topographically but differ in terms of geographical location, along with a slightly higher mean elevation for class 8. Finally, class 9 corresponds to water bodies.

Overall, the results of the k-means classification allowed highlighting three major groups of landforms that are often found geographically associated. The first group is the mountainous ensemble, which differentiated through elevation, class 11 having a much higher altitude (933 m a.s.l., Table 3) than class 12 (540 m a.s.l., Table 3). The class 2 "Foothills" with an elevation of 389 m a.s.l. encircles this mountainous ensemble and marks the transition towards class 10 "Low hills and plateaus". The second group is represented by wet and floodable plains in which moisture index (HAND) makes it possible to separate classes 1 and 5; class 1 being more often flooded (HAND = 9.21, Table 3) than class 5 (HAND = 17.64, Table 3). The last major group entails classes 3 and 8 as coastal and interior plains respectively in which elevation and moisture index are the main discriminating criteria.

3.3 Interpreting the mapped landform units

The 12 landform classes of our final map (Fig. 5) can be interpreted in terms of geomorphological meaning together with some hydrological and/or pedological attributes. First, Class 1 "low wet plains" (dark blue) is mainly located in the Congo Basin *stricto sensu*. These core wetlands correspond to the lower altitudes of the inner plains of the basin occupied by flooded swamp forests with peat soils and traversed by slowly flowing rivers of the Congo watershed (Bwangoy et al. 2010). They are very similar to the *low-várzea* areas of Brazilian Amazonia, which correspond to inundated forests, either permanently or seasonally (Wittmann et al. 2004). Class 5 of our map belongs to the same group of inundated

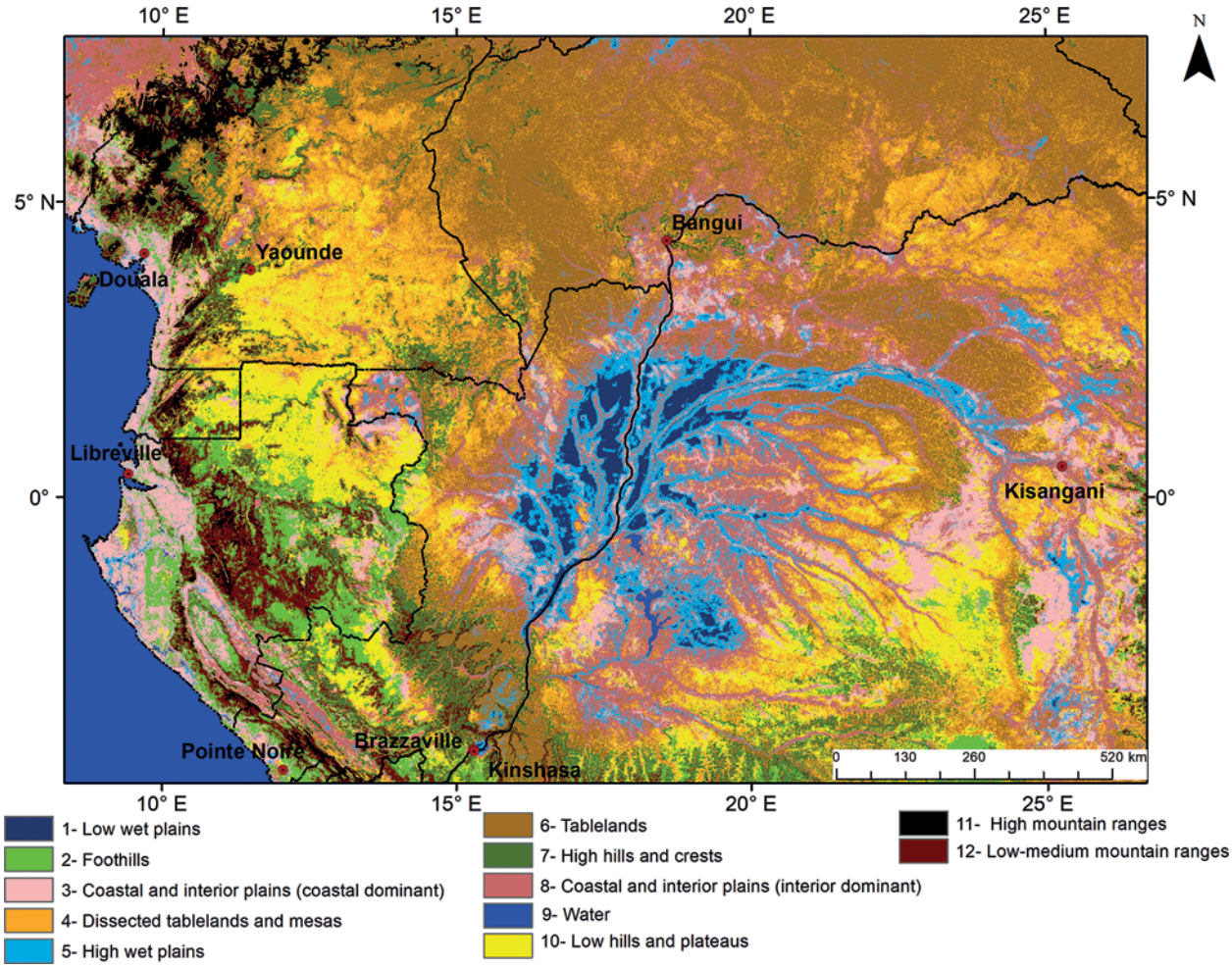

Fig. 5. Final map of landform classes of the Congo Basin and adjacent regions at 900 m of spatial resolution.

landforms ("high wet plains": light blue) but it occupies areas of slightly higher elevation in the landscape (Table 3), in a way comparable to the *high-várzea* forests of Amazonia only subjected to higher flood levels. Smaller wetlands have also been detected outside the "Cuvette Centrale", such as in northwestern Congo, west of a watershed between the Ogooué basin and the Congo basin, where a flat piedmont surface is seasonally waterlogged (Unit 7.4 "Swampy plains" in (Schwartz & Namri 2002). Non-inundated lowlands, equivalent to the *terra firme* rainforest domain of Amazonia, are represented at the periphery of the Central Congo wetlands (class 8, in dark beige). These interior plains are mainly accumulation surfaces filled with fluviatile and/or lacustrine sediments of Plio-Quaternary age, but they also include low-relief erosional surfaces like the karstic plains of the Oubangian piedmont (Mbaïki region, west of Bangui) and that of the Niari-Nyanga synclinorium (at the foot of the Chaillu mountains) as well as some very flat crystalline plains strewn with small inselbergs. Toward the sea, similar plains, locally underlain by laterite-capped terrigenous red beds (*série des cirques*: Giresse & Le Ribault 1981), make a smooth transition with coastal plains of fluvio-marine origin and Quaternary age, mainly represented in class 3 (light beige). These coastal plains include both non-floodable and floodable areas (not all depicted at this scale).

Higher in the topography are the multiconvex landscapes of "low hills and plateaus" (class 10, in yellow), mainly shaped from highly weathered rocks of the granite-gneiss complexes of Precambrian age – a landform unit well represented in southern Cameroon and northern Gabon. This monotonous surface of moderate elevation (500–700 m a.s.l.), typified by repeated patterns of convex hills ("half-oranges") and locally dominated by rocky domes, corresponds to the "*surface intérieure*"

described by Segalen (1967) in southern Cameroon. Toward the East, this topographic surface makes a transition with "dissected tablelands and mesas" (class 4, in orange) belonging to the "*surface centrafricaine*" on the territory of Central African Republic (Boulvert 1996), as part of the wider continent-scale "African Surface" (Burke & Gunnell 2008). Such eroded tablelands are often lateritic mesas developed from mafic basement rocks (gabbro, dolerite) above degraded, rolling "etch" surfaces that expose the weathering front. Other elevated areas of the Congo Basin margins are the large sandstone plateaus crowning the "*surface centrafricaine*" to the North (Carnot-Gadzi and Mouka-Ouadda plateaus) and adjoining the Mayombé mountains to the Southwest (Batéké plateaus): all of them coincide with the class 6 of our landform map (unit "tablelands", in light brown). Closely associated with the Batéké plateaus is a unit of "high hills and crests" (class 7, in dark green) which correspond here to dissected areas located at the foot and south-west of the sandstone caprock. This unit occurs in other parts of the study area where it usually forms a system of Appalachian-like ridges and valleys shaped by differential erosion in alternating quartzite-schist folded bands (southernmost Cameroon, southeastern Central African Republic). The highest reliefs of the study area are found to the West, where they constitute a quasi-continuous N-S trending mountain range forming a marginal swell on the western flank of the Congo Basin (Burke & Gunnell 2008, Petit 1990). It includes low- and medium-elevation mountain ranges (i.e., class 12, in dark brown) like the Chaillu and Mayombé massifs (600–1,200 m a.s.l.) together with the west-facing escarpments bounding the "*surface intérieure*" of Cameroon and other inner scarps. It also comprises the highest mountains and volcano-capped swells of the Cameroon Volcanic Line (i.e., "High mountain ranges" for class 11, in black), displaying the highest average values of altitude, slope, dissection and roughness (Table 3). The last landform unit (class 2, in light green) encompasses an intermediate landscape of foothills at the interface between mountains and dissected tablelands, hilly areas or coastal plains – a unit well represented around the Chaillu and Mayombé massifs.

3.4 Comparing with existing maps

At fine scale in South of Cameroon (1:500 000), and despite the detailed typology of the morphopedological map of Vallerie (1995), the comparison with our map is rather consistent (Appendix A). Logically, we note strong agreement between our landscape units relating to mountains (classes 2, 7, 11, 12) and Vallerie's classes relating to similar situations ("Residual reliefs", "high complex hills", "convex hill with narrow valley", "relatively rugged hill"). We also note large agreement between two of our units linked to plains (classes 5, 8) and the "Small low hill or slightly undulating plateau", "Plain" and "Convex hill or plain" Vallerie's classes, while the third unit (class 3) matches only with the "Plain" Vallerie's class. Our most extensive unit 10, made of the multiconvex landscapes of "Low hills and plateau", also matches with the most extended Vallerie's class "Hill with heavily/widely undulating plateaus". Despite these agreements, we note that our landscape units relating to tablelands (classes 4, 6), including our second most represented class "Dissected tablelands", were dispatched into different Vallerie's classes that have little connection with tablelands. This reflects the fact that Vallerie has not defined any typical tableland-related landscapes.

At a medium scale (1:1 000 000), our classification and the geomorphological map of the Central African Republic (Boulvert 1996) appeared consistent (Table 4, Fig. 6). We note strong agreement between our most extended unit 6 "Tablelands" and Boulvert's classes ("Scarp with concave shape", "Interfluves of the sandstone plateau" "Valleys of the sandstone plateau") that specify the different landscape subunits of these "Tablelands". We note large agreement between our landscape units relating to high hills and crests (7) and the two Boulvert's classes relating to similar situations ("Scarp with convex shape", "Scarp with concave shape"). We also note large agreement between three of our units linked to plains and water (classes 3, 5, 8) and the "Piedmont surface", "Alluvium-Filled Valleys", and "Water" Boulvert's classes. Surprisingly, we did not find any significant agreement between our units linked to water and "Water" Boulvert's class. We note that the most extended Boulvert's class (i.e. "Centrafrican surface") is distributed in three of our classes (4, 7, 10). This reflects the fact that Boulvert (1996) had grouped together different landscape units in this class, such as dissected tablelands, multiconvex low hills, and high hills and crests.

At a larger scale (1:2 000 000), our classification and the geomorphological map of the Gabon (Martin et al. 1981) appeared also consistent (Appendix B). Logically, we note strong agreement between our landscape units relating to mountains and their foothills (classes 2, 11, 12) and Martin's classes relating to similar situations ("Lambarene, Koumouna and Mayombe mountains", "Crystal and Ndjole mountains", "Chaillu mountains"). We also note large agreement between our units linked to water and plains (classes 1, 3, 5, 8, 9) and the "Coastal sedimentary basin" and "Ngounie-Nynaga synclinal" Martin's classes. Our second most extended unit 10, which are the multiconvex landscapes of "Low hills and plateau", also matches with the most extended Martin's class "Northern and northeastern plateaus".

Table 4. Cross-classification table showing the comparison between our landform map and the geomorphological map of Central African Republic by Boulvert (1996). Corrected frequencies are expected to be around zero in case of independence between rows and columns, while a positive departure in a cell indicates association between the corresponding cells and vice versa for a negative departure. CvxS: Convex Scarp, CcvS: Concave Scarp, ISP: Interfluves of Sandstone Plateaus, VSP: Valleys of Sandstone Plateaus, CS: Centrafrican Surface, LM: Lateritic Mesas; BL: Basement Landforms, AFV: Alluvium-Filled Valleys, PS: Piedmont Surface. * = significant p-value for positive corrected frequencies of Chi-square by cell test

Present study		**Geomorphological units in Central African Republic, Boulvert (1996)**										
Class	**Landform units**	**CvxS**	**CcvS**	**ISP**	**VSP**	**CS**	**LM**	**BM**	**AFV**	**Water**	**PS**	**% area**
7	High hills and crests	6.26*	2.01*	-0.82		0.46*	-0.23	-0.28	-1.00	-0.96	-0.97	7.03
12	Low-medium mountain ranges edges	8.07*	-1.00	-0.99	-0.96	0.67	-0.65	-1.00	-1.00	-0.97	-0.82	0.41 Coastal and interior plains (coastal dominant)
6	Tablelands	-0.51	0.19*	0.62*	0.22*	-0.17	0.09	-0.49	-0.78	-0.75	-0.72	54.96
2	Foothills	3.31	-1.00	-1.00	-1.00	1.14	-1.00	-1.00	-1.00	-0.52	-0.93	0.15
4	Dissected tablelands	-0.21	-0.44	-0.63	0.09*	0.65*	0.14*	1.75*	0.40*	-0.36	-0.63	19.86
10	Low hills and plateaus	-0.49	-0.93	-0.86	0.06	0.24*	-0.71	2.19	3.33*	1.75*	0.60*	1.83
8	Coastal and interior plains (interior dominant)	-0.93	-0.83	-0.87	-0.60	-0.38	-0.14	-0.49	2.25*	3.17*	3.12*	12.22
5	High wet plains	-0.99	-1.00	-0.84	-0.67	-0.89	-0.61	-1.00	4.00*	2.03*	6.66*	1.98
1	Low wet plains	-1.00	-1.00	-1.00	-1.00	-0.76	-1.00	-1.00	-1.00	6.57	3.49	0.01
3	Coastal and interior plains (coastal dominant)	-1.00	-1.00	-1.00	-0.97	-0.96	-0.88	-0.74	0.57*	6.23*	4.49*	1.55
	(coastal dominant)											
9	Water	-1.00	-1.00	-1.00	-1.00	-1.00	-1.00	-1.00	-1.00	11.14	0.54	0.01
	%area	3.76	1.28	27.72	9.58	37.27	4.14	0.42	0.53	7.21	8.10	100.00

At the Cuvette Centrale wetlands in the Congo basin, our classification and the probability map of vegetation types (Dargie et al. 2017, scale at 1:9 000 000) appeared consistent (Appendix C). Logically, we note strong agreement between our landscape units relating to low/high wet plains (classes 1, 5) and Dargie's classes relating to swamps ("Hardwood swamp" and "Palm-dominated swamp"), and water or savanna. We also note that the most extended Dargie's class (i.e. "Terra firme forest") is distributed in most of our classes (2, 3, 4, 6, 7, 10) outside the water and wet plains. This Dargie's class is relatively less distributed in our class 8 that we interpreted as non-inundated lowlands of savanna or forest and which indeed display rather balanced areas of these two vegetation types (see below).

The global scale topography 18-fold classification of Iwahashi and Pike (2007) at scale of 1:100 000 000 also agrees with our classification (Appendix D). For example, we note a large agreement between, on the one hand, our landscape units relating to low/high wet plains (classes 1, 5) and Iwahashi and Pike's classes relating to gentle slope and, on the other hand, our landscape units relating to mountains (classes 7, 11, 12) and Iwahashi and Pike's classes relating to steep slopes.

3.5 Possible influences of forest-savanna mosaics

A first subset of our classes showed overwhelming dominance of a single vegetation type (most frequently forest, classes 1, 2, 3, 5 and 10), but also grassland (class 9) that precludes significant impact of vegetation height variability on our morphometric analysis (Appendix F). Among the classes that displayed both forest (high cover) and savanna vegetation (intermediate cover), we found several of them related to mountains and crests (classes 7, 11, 12) or tablelands either dissected (class 4) or not (class 6). Having the distinctive criteria of these classes (e.g., high average elevation, dissection amplitude) being affected by vegetation height variations of 40 m or less is unlikely. Only class 8 ('Coastal and interior plains (interior dominant)') simultaneously entailed savanna and forest vegetation along with geomorphic signatures liable of being biased by vegetation height. Also singling out this class was the difficulty to separate floodable and non-floodable areas in a context of low relief energy. Class 8 is thus to remain under scrutiny, but apart from it, this analysis indicates that biases resulting from canopy variations are likely to be of limited influence on the quality of the final map.

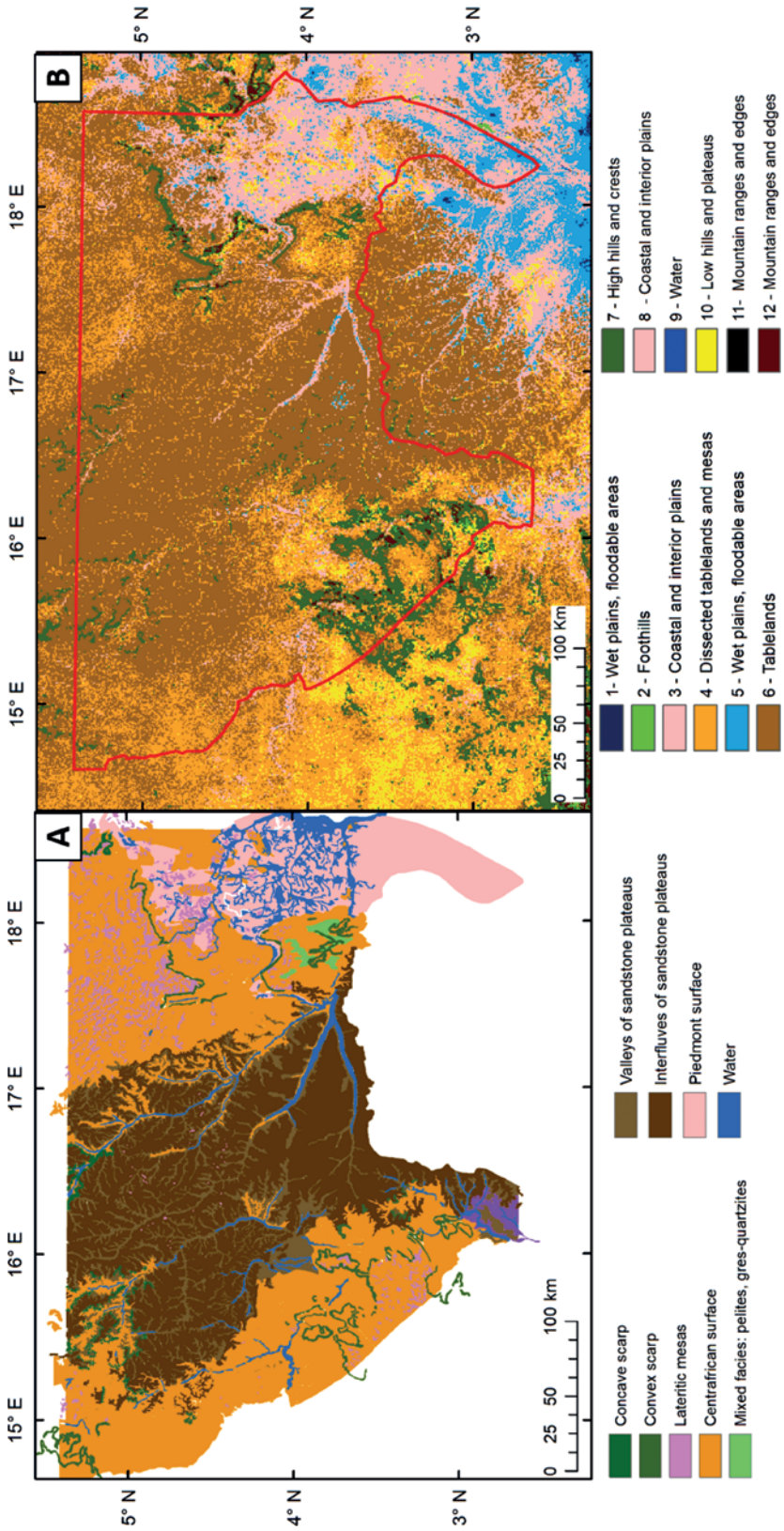

Fig. 6. Comparison between the geomorphological map of Central African Republic **(A)** by Boulvert (1996) and our landform map **(B)** in a small area centered on the Carnot-Gadzi plateau, west of Bangui.

4 Discussion

The method used in this paper heavily relied on a two-scale textural analysis of Fourier 2D periodograms through the r-spectra (FOTO) method (Couteron et al. 2006) which confirmed here its effectiveness for landform depiction and mapping at very large (subcontinental) scales after the regional mapping of (Bugnicourt et al. 2018). A drawback commonly attributed to automated, geomorphometric analysis based on DEM datasets is the a priori definition of window size for the derivation of morphometric variables (Józsa & Fábián 2016). The size of the window determines the scale of the mapping and the overall detection of landforms, with a risk of generalization of smaller surface details or the elimination of larger landform elements, so changing the extent of window size can completely change the output results. In our methodology, we proceeded with a multi-scale processing of SRTM data, with two contrasted window sizes (*ca* 1 km and *ca* 10 km), when applying the textural analysis through Fourier 2D periodograms. Their spatial combination allowed the definition of new synthetic variables that summarize textural variation beyond any scale dependency. In spite of an important contrast in window size, we found inter-correlated texture features (FOTO PCA scores) between the two scales that thus appeared as robust, synthetic geomorphic signatures, with limited dependence on window size. Such texture features directly underlain one of the two main gradients (vertical axis in Fig. 4C) expressed in our map that opposed classes having textures with strong contributions of intermediate grain (top, Fig. 4C; hump-shaped spectra in Fig. 3) to those with heterogeneous textures (bottom; straight spectra in Fig. 3). Illustrations provided in Fig. 3 make apparent that the largest window size is overall more efficient to distinguish between patterns, though the smaller size may be more accurate to depict fine-grained textures characterizing certain classes.

The major advantage of the textural analysis is that it offers the opportunity to characterize "geometric signatures" (Pike 1988) conducive to the identification of "landform types" (MacMillan et al. 2000). Therefore, the method directly permitted the detection of landform assemblages (for example, hilly landscapes), and bypassed the delineation of elementary forms (e.g., individual hills). Through r-spectra shapes (e.g. in log-log scaling, Fig. 3) it also provides characteristics of certain families of landform assemblages. In both Bugnicourt et al. (2018), and the present study, multi-convex assemblages displayed humped shaped-spectra that point towards ranges of characteristics wavelengths, while spectra from mountainous systems and dissected tablelands tended to be straighter reflecting intricate patterns of very variable sizes that are barely distinguishable from self-similarity. There is thus a potential for comparison and generalization between geographic regions.

However, a DEM resolution of ~30 m did not allow the detection of landform types of minor extent such as tidal plains covered with riparian mangrove fringe, which were difficult to separate from the rest of the coastal plains. The lack of topographic variation in such configurations of low-altitude plains is a classical problem in general geomorphometry (Evans 2012). In the Congo Basin, this difficulty was pointed by Bwangoy et al. (2010) in their attempt to discriminate the wetland areas from non-inundated (*terra firme*) lowlands. The same difficulty arises from our work in local situations of very low relief topography (coastal areas, central basin), despite the use of a specific index (HAND index: Rennó et al. 2008) in order to discriminate wetlands and non-wetlands. This difficulty is partially a scale-dependent problem, because the SRTM DEM is probably too coarser in spatial and vertical resolution to detect minor elevation changes. Moreover, strong spatial variations in vegetation height can easily blur such small changes. But it appeared in our case that savanna-forest landscapes are barely notable in about half of our classes, which are mainly covered by close canopy forests. Such mosaic landscapes also seem unlikely significantly biasing the geomorphic signatures of most of the remaining classes, which relate to ranges of elevation variability clearly above maximal contrast in vegetation height. Only one class among 12 (#8, 'Coastal and interior plains (interior dominant)') is to remain under scrutiny as liable to be locally affected by forest-savanna landscapes in some of the areas where we detected it. However, we can overall consider that canopy variation is probably of low influence on the geomorphic features at the grain size we used, especially when applying the textural analysis (window sizes of 1 km and 10 km).

Despite these limitations related to the coarse resolution of the SRTM data and to the macroscopic scale of our mapping, we globally noted a good agreement for categories relating to wetlands with existing maps of greater resolution and smaller extents, including the coastal areas of Cameroon and Gabon where our floodable units are largely reminiscent of mapped vegetation wetlands (Aldous et al. 2020) though our map logically provides coarser outlines. More broadly, we were able to verify the working hypothesis that our landform map is able to retrieve the main interpretable geomorphic features of the different existing maps despite their varying aims and methods. The observed differences mainly depend on the map resolution and the typology adopted in the legend classification given rise to landform classes with different names and spatial extents. They also appear where an author emphasized an aspect that has no direct expression in geomorphometry (e.g. geology) or

for units that merge heterogeneous landforms (e.g. Boulvert's Centrafrican surface).

Various applications may directly arise from our automatic method of landform classification and mapping. In the field of pedology, it could serve as a strong basis for predicting and mapping soil units at the landscape scale, given the close soil-landform imbrications and interactions at the *catena* level (Birkeland 1999, Gerrard 1992, Schaetzl & Anderson 2005). Geomorphology is acknowledged as a proxy for soil properties because it incorporates the combined effects of geology, climate and erosion on soil development (Guitet et al. 2015b). In fact, several of extant maps used landforms as proxies for soil *catenas* or for dominant soil types. Comparison with these existing maps (Table 4, Appendices A to D) indicated a strong correlation between our landform units and the soil units depicted on the basis of expert-based geomorphological analyses. With the help of automated processing of freely available data (SRTM DEM), our method may offer an alternative to the time-consuming, rather subjective task of manual mapping and/or aerial photointerpretation of landforms beneath canopy, in order to prepare robust soil maps at large or regional scales. In the broader scope of biological conservation aims and strategies, our method of landform depiction could also be applicable for predicting biodiversity metrics and patterns, since it is widely accepted that geomorphodiversity underpins biodiversity (Burnett et al. 1998, Nichols et al. 1998, Tukiainen et al. 2019) and modulates forest structure properties (Gourlet-Fleury et al. 2011, Guitet et al. 2015a). Moreover, particular landform systems that reflect tectonic and climate stability are known to harbor specific biodiversity patterns (Guitet et al. 2016, Hammond 2005). These results obtained in the neotropics deserve further investigation in Africa.

5 Conclusion

The initially stated aim of this research was to test an adapted version of the automatic method proposed by Bugnicourt et al. (2018), in order to classify and to map landforms in a very large area (i.e. subcontinental scale) centered on the Congo Basin, Central Africa. Results from this study demonstrate the usefulness of a combined approach involving texture analysis (FOTO method) and morphometric calculations, with the SRTM dataset serving as input for deriving Fourier r-spectra and topographic indices. Our cartographic results match the main patterns of existing geomorphological maps and classifications, and the statistical evaluation indicates that most of our landform classes share the interpretations of expert-mapped units at different scales. In order to better discriminate wetlands and non-wetlands in local contexts of very low relief such as the coastal areas or the inner central basin, further investigations based on finer-resolution DEM and some hydrological metrics will be necessary for producing more precise maps of floodable areas. Future work will also be dedicated to the inclusion of the landform map results into wider objectives of using environmental predictors to infer soil units, forest types, forest structure, forest biomass and carbon storage at the scale of the whole Congo Basin.

An interesting prospect to improved applications of the method is the release of recent global databases on earth surface altimetry, notably ALOS World 3D (https://portal.opentopography.org/raster?opentopoID=OTALOS.112016.4326.2, acces date: May 24th 2021) which is reported as more reliable than the SRTM, specifically, for deriving hydrological networks and indices of the HAND type (Courty et al. 2019), even though ALOS World 3D is also a DSM and not a DTM.

So far, our method has been applied and tested in two different areas of the humid tropics, in the Eastern Guiana shield (Bugnicourt et al. 2018) and in Central Africa (this study). We believe our method is sufficiently generic to help with most landform systems on Earth since it built and developed in accordance with the fundamental idea of Iwahashi & Pyke (2007) that automatically extracted texture information is useful for global mapping of landforms. We however acknowledge that most of our experience is thus far centered on old cratons in tropical regions where mountain systems are quite marginal. Addressing low-relief regions in other morphoclimatic zones (e.g. cold regions: Patagonia, Scandinavia) or younger relief systems may request adapting window sizes for texture or refining some of the geomorphic criteria.

Acknowledgements: This work is part of the International Joint Laboratory "DYnamics of land eCOsystems in Central Africa in a context of global changes: IJL DYCOFAC". The mapping presented in this paper is part of the 3DFORMOD project 'Combining remote sensing and 3D forest modelling to improve tropical forests monitoring of GHG emissions' (EU-H2020 – FACCE ERA-GAS, grant agreement No 696356). We also acknowledge synergies with the DynAfFor project supported by a French Fund for the Global Environment (grant numbers Nos. CZZ1636.01D and CZZ1636.02D).

References

Aldous, A., Schill, S., Raber, G., Paiz, M. C., Mambela, E., & Stévart, T. (2020). Mapping complex coastal wetland mosaics in Gabon for informed ecosystem management: Use of object-based classification. *Remote Sensing in Ecology and Conservation*, *7*(1), 64–79.https://doi.org/10.1002/rse2.161

Amatulli, G., Domisch, S., Tuanmu, M.-N., Parmentier, B., Ranipeta, A., Malczyk, J., & Jetz, W. (2018). A suite of global, cross-scale topographic variables for environmental and biodiversity modeling. *Scientific Data, 5*(1), 180040. https://doi.org/10.1038/sdata.2018.40

Bétard, F., & Bourgeon, G. (2009). Cartographie morphopédologique: De l'évaluation des terres à la recherche en géomorphologie. Géomorphologie Relief Processus *Environnement, 15*, 187–198.

Birkeland, P. W. (1999). *Soils and geomorphology*. New York: Oxford University Press.

Boulvert, Y. (1996). *Etude géomorphologique de la République Centrafricaine: carte à 1/1000000 en deux feuilles Ouest et Est.*

Bourgine, B., & Baghdadi, N. (2005). Assessment of C-band SRTM DEM in a dense equatorial forest zone. *Comptes Rendus Geoscience, 337*(14), 1225–1234. https://doi.org/10.1016/j.crte.2005.06.006

Bugnicourt, P., Guitet, S., Santos, V. F., Blanc, L., Sotta, E. D., Barbier, N., & Couteron, P. (2018). Using textural analysis for regional landform and landscape mapping, Eastern Guiana Shield. *Geomorphology, 317*, 23–44. https://doi.org/10.1016/j.geomorph.2018.03.017

Burke, K. (2001). Origin of the Cameroon line of volcano-capped swells. *The Journal of Geology, 109*(3), 349–362. https://doi.org/10.1086/319977

Burke, K., & Gunnell, Y. (2008). The African erosion surface: A continental-scale synthesis of geomorphology, tectonics, and environmental change over the past 180 million years. *Geological Society of America, 201*, 1–66. https://doi.org/10.1130/2008.1201

Burnett, M. R., August, P. V., Brown, J. H., & Killingbeck, K. T. (1998). The influence of geomorphological heterogeneity on biodiversity I. A patch-scale perspective. *Conservation Biology, 12*(2), 363–370. https://doi.org/10.1046/j.1523-1739.1998.96238.x

Bwangoy, J.-R. B., Hansen, M. C., Roy, D. P., De Grandi, G., & Justice, C. O. (2010). Wetland mapping in the Congo Basin using optical and radar remotely sensed data and derived topographical indices. *Remote Sensing of Environment, 114*(1), 73–86. https://doi.org/10.1016/j.rse.2009.08.004

Courty, L. G., Soriano-Monzalvo, J., & Pedrozo-Acuna, A. (2019). Evaluation of open-access global digital elevation models (AW3D30, SRTM, and ASTER) for flood modelling purposes. *Journal of Flood Risk Management, 12*(S1), e12550. https://doi.org/10.1111/jfr3.12550

Couteron, P. (2002). Quantifying change in patterned semi-arid vegetation by Fourier analysis of digitized aerial photographs. *International Journal of Remote Sensing, 23*(17), 3407–3425. https://doi.org/10.1080/01431160110107699

Couteron, P., Barbier, N., & Gautier, D. (2006). Textural ordination based on Fourier spectral decomposition: A method to analyze and compare landscape patterns. *Landscape Ecology, 21*(4), 555–567. https://doi.org/10.1007/s10980-005-2166-6

Dargie, G. C., Lewis, S. L., Lawson, I. T., Mitchard, E. T., Page, S. E., Bocko, Y. E., & Ifo, S. A. (2017). Age, extent and carbon storage of the central Congo Basin peatland complex. *Nature, 542*(7639), 86–90. https://doi.org/10.1038/nature21048

De Matos-Machado, R., Toumazet, J.-P., Bergès, J.-C., Amat, J.-P., Arnaud-Fassetta, G., Bétard, F., … Jacquemot, S. (2019). War landform mapping and classification on the Verdun battlefield (France) using airborne LiDAR and multivariate analysis. *Earth Surface Processes and Landforms, 44*(7), 1430–1448. https://doi.org/10.1002/esp.4586

Drăguţ, L., & Eisank, C. (2012). Automated object-based classification of topography from SRTM data. *Geomorphology, 141*, 21–33. https://doi.org/10.1016/j.geomorph.2011.12.001

Evans, I. S. (2012). Geomorphometry and landform mapping: What is a landform? *Geomorphology, 137*(1), 94–106. https://doi.org/10.1016/j.geomorph.2010.09.029

Farr, T. G., Rosen, P. A., Caro, E., Crippen, R., Duren, R., Hensley, S., … Roth, L. (2007). The shuttle radar topography mission. *Reviews of Geophysics,* 45(2).

Fayolle, A., Engelbrecht, B., Freycon, V., Mortier, F., Swaine, M., Réjou-Méchain, M., … Gourlet-Fleury, S. (2012). Geological substrates shape tree species and trait distributions in African moist forests. *PLoS One, 7*(8), e42381. https://doi.org/10.1371/journal.pone.0042381

Fayolle, A., Swaine, M. D., Bastin, J.-F., Bourland, N., Comiskey, J. A., Dauby, G., … Plumptre, A. J. (2014). Patterns of tree species composition across tropical African forests. *Journal of Biogeography, 41*(12), 2320–2331. https://doi.org/10.1111/jbi.12382

Figueiredo, F. O., Costa, F. R., Nelson, B. W., & Pimentel, T. P. (2014). Validating forest types based on geological and landform features in central Amazonia. *Journal of Vegetation Science, 25*(1), 198–212. https://doi.org/10.1111/jvs.12078

Gerrard, J. (1992). Soil geomorphology: an integration of pedology and geomorphology. London: Chapman and Hall.

Giresse, P. (2005). Mesozoic–Cenozoic history of the Congo basin. *Journal of African Earth Sciences, 43*(1-3), 301–315. https://doi.org/10.1016/j.jafrearsci.2005.07.009

Giresse, P., & Le Ribault, L. (1981). Contribution de l'étude exoscopique des quartz à la reconstitution paléogéographique des derniers épisodes du Quaternaire littoral du Congo. *Quaternary Research, 15*(1), 86–100. https://doi.org/10.1016/0033-5894(81)90116-2

Gourlet-Fleury, S., Rossi, V., Rejou-Mechain, M., Freycon, V., Fayolle, A., Saint-André, L., … Picard, N. (2011). Environmental filtering of dense-wooded species controls above-ground biomass stored in African moist forests. *Journal of Ecology, 99*(4), 981–990. https://doi.org/10.1111/j.1365-2745.2011.01829.x

Guitet, S., Freycon, V., Brunaux, O., Pélissier, R., Sabatier, D., & Couteron, P. (2016). Geomorphic control of rain-forest floristic composition in French Guiana: More than a soil filtering effect? *Journal of Tropical Ecology, 32*(1), 22–40. https://doi.org/10.1017/S0266467415000620

Guitet, S., Herault, B., Molto, Q., Brunaux, O., & Couteron, P. (2015a). Spatial structure of above-ground biomass limits accuracy of carbon mapping in rainforest but large scale forest inventories can help to overcome. *PLoS One, 10*(9), e0138456. https://doi.org/10.1371/journal.pone.0138456

Guitet, S., Pélissier, R., Brunaux, O., Jaouen, G., & Sabatier, D. (2015b). Geomorphological landscape features explain floristic patterns in French Guiana rainforest. *Biodiversity and*

Conservation, 24(5), 1215–1237. https://doi.org/10.1007/s10531-014-0854-8

Hammond, D. S. (2005). Guianan forest dynamics: geomorphological control and tropical forest change across diverging landscapes. In D.S. Hammond (eds.),Tropical forests of the Guiana shield: ancient forests in a modern world (p. 343–379). CABI Publ. Wallingford UK, https://doi.org/10.1079/9780851995366.0343

Iwahashi, J., & Pike, R. J. (2007). Automated classifications of topography from DEMs by an unsupervised nested-means algorithm and a three-part geometric signature. *Geomorphology, 86*(3-4), 409–440. https://doi.org/10.1016/j.geomorph.2006.09.012

Józsa, E., & Fábián, S. Á. (2016). Mapping landforms and geomorphological landscapes of Hungary using GIS techniques. *Studia Geomorphologica Carpatho-Balcanica, 50*, 19–31.

Leroux, M. (2001). *The meteorology and climate of tropical Africa*. Springer Science & Business Media.

MacMillan, R. A., Pettapiece, W. W., Nolan, S. C., & Goddard, T. W. (2000). A generic procedure for automatically segmenting landforms into landform elements using DEMs, heuristic rules and fuzzy logic. *Fuzzy Sets and Systems, 113*(1), 81–109. https://doi.org/10.1016/S0165-0114(99)00014-7

Manly, B. F., & Alberto, J. A. N. (2016). *Multivariate statistical methods: a primer*. Chapman and Hall/CRC. https://doi.org/10.1201/9781315382135

Martin, D., Chatelin, Y., Collinet, J., Guichard, E., Sala, G.-H., & Le Rouget, G. (1981). *Les sols du Gabon: pedogenese, repartition et aptitudes: cartes a 1: 2.000. 000.*

Milesi, J. P., Toteu, S. F., Deschamps, Y., Feybesse, J. L., Lerouge, C., Cocherie, A., … Cailteux, J. (2006). An overview of the geology and major ore deposits of Central Africa: Explanatory note for the 1: 4,000,000 map "Geology and major ore deposits of Central Africa.". *Journal of African Earth Sciences, 44*(4-5), 571–595. https://doi.org/10.1016/j.jafrearsci.2005.10.016

Moudrý, V., Lecours, V., Gdulová, K., Gábor, L., Moudrá, L., Kropáček, J., & Wild, J. (2018). On the use of global DEMs in ecological modelling and the accuracy of new bare-earth DEMs. *Ecological Modelling, 383*, 3–9. https://doi.org/10.1016/j.ecolmodel.2018.05.006

Nichols, W. F., Killingbeck, K. T., & August, P. V. (1998). The influence of geomorphological heterogeneity on biodiversity II. A landscape perspective. *Conservation Biology, 12*(2), 371–379. https://doi.org/10.1046/j.1523-1739.1998.96237.x

Ortuño, M., Guinau, M., Calvet, J., Furdada, G., Bordonau, J., Ruiz, A., & Camafort, M. (2017). Potential of airborne LiDAR data analysis to detect subtle landforms of slope failure: Portainé, Central Pyrenees. *Geomorphology, 295*, 364–382. https://doi.org/10.1016/j.geomorph.2017.07.015

Panizza, M. (2009). The geomorphodiversity of the Dolomites (Italy): A key of geoheritage assessment. *Geoheritage, 1*(1), 33–42. https://doi.org/10.1007/s12371-009-0003-z

Petit, M. (1990). *Les grands traits morphologiques de l'Afrique centrale atlantique*. Paysages Quat. L'Afrique Cent. Atl. Off. Rech Sci Tech O.-M. ORSTOM, Paris, p. 20–30.

Pike, R. J. (1988). The geometric signature: Quantifying landslide-terrain types from digital elevation models. *Mathematical Geology, 20*(5), 491–511. https://doi.org/10.1007/BF00890333

Pike, R. J., Evans, I. S., & Hengl, T. (2009). Geomorphometry: A brief guide. Developments in Soil Science, 33, 3–30.

Proisy, C., Couteron, P., & Fromard, F. (2007). Predicting and mapping mangrove biomass from canopy grain analysis using Fourier-based textural ordination of IKONOS images. *Remote Sensing of Environment, 109*(3), 379–392. https://doi.org/10.1016/j.rse.2007.01.009

Réjou-Méchain, M., Pélissier, R., Gourlet-Fleury, S., Couteron, P., Nasi, R., & Thompson, J. D. (2008). Regional variation in tropical forest tree species composition in the Central African Republic: An assessment based on inventories by forest companies. *Journal of Tropical Ecology, 24*(6), 663–674. https://doi.org/10.1017/S0266467408005506

Rennó, C. D., Nobre, A. D., Cuartas, L. A., Soares, J. V., Hodnett, M. G., Tomasella, J., & Waterloo, M. J. (2008). HAND, a new terrain descriptor using SRTM-DEM: Mapping terra-firme rainforest environments in Amazonia. *Remote Sensing of Environment, 112*(9), 3469–3481. https://doi.org/10.1016/j.rse.2008.03.018

Schaetzl, R., & Anderson, S. (2005). *Soils: Genesis and Geomorphology*. Cambridge: Cambridge University Press. https://doi.org/10.1017/CBO9780511815560

Schwartz, D., & Namri, M. (2002). Mapping the total organic carbon in the soils of the Congo. *Global and Planetary Change, 33*(1-2), 77–93. https://doi.org/10.1016/S0921-8181(02)00063-2

Sokal, R. R., & Rohlf, F. J. (1981). *Biometry: the principles and practice of statistics in biological research*.

Tukiainen, H., Kiuttu, M., Kalliola, R., Alahuhta, J., & Hjort, J. (2019). Landforms contribute to plant biodiversity at alpha, beta and gamma levels. *Journal of Biogeography, 46*(8), 1699–1710. https://doi.org/10.1111/jbi.13569

Vallerie, M. (1995). *CAMEROUN, SUD – PÉDOLOGIE*. 1:500000. Atlas régional Sud-Cameroun.

Verbeeck, H., Boeckx, P., & Steppe, K. (2011). Tropical forests: Include Congo basin. *Nature, 479*(7372), 179. https://doi.org/10.1038/479179b

Wittmann, F., Junk, W. J., & Piedade, M. T. (2004). The várzea forests in Amazonia: Flooding and the highly dynamic geomorphology interact with natural forest succession. *Forest Ecology and Management, 196*(2-3), 199–212. https://doi.org/10.1016/j.foreco.2004.02.060

Manuscript received: December 23, 2021
Revisions requested: April 14, 2022
Revised version received: May 25, 2022
Accepted: June 2, 2022

Appendices

Appendix A. Cross-classification table with computation of corrected frequencies for comparison between our landform map and the soil map of South Cameroon by Vallerie (1995). CHNV: Convex Hill with Narrow Valley, HUP: Hill with heavily/widely Undulating Plateaus, MUH: Moderately Undulating Hill, VGUP: Very Gently Undulating Plain, SLH: Small Low Hill, SUP: Slightly Undulating Plateau; * = significant p-value for positive corrected frequencies of Chi-square by cell test; Classes 1 (low wet plains) and 9 (water) of our map do not appear within the area covered by Vallerie's map.

Present study		**Soil mapping units in Southern Cameroon, Vallerie (1995)**											
Class	**Landform units**	**Residual relief**	**High complex hills**	**CHNV**	**Relatively rugged hill**	**HUP**	**Hill or plain**	**MUH**	**VGUP**	**Convex hill or plain**	**SLH or SUP**	**Plain**	**% area**
12	Low-medium mountain ranges	11.52*	5.62*	0.36*	0.78*	-0.48	-0.70	-0.97	-0.90	-1.00	-0.94	-0.99	3.45
11	High mountain ranges	0.91*	4.30	-0.01	-1.00	-0.02	-1.00	-1.00	-1.00	-1.00	-1.00	-1.00	0.33
7	High hills and crests	2.34*	2.28*	0.35*	3.11*	-0.18	-0.50	-0.19	-0.55	-0.79	-0.83	-0.93	12.64
2	Foothills	1.78*	1.54*	0.77*	0.90*	0.05	-0.70	-0.72	-0.92	-1.00	-1.00	-1.00	1.28
10	Low hills and plateaus	-0.94	-0.66	-0.05	-0.75	0.24*	-0.18	-0.27	-0.09	-0.73	-0.76	-0.88	41.29
4	Dissected tablelands	-0.79	-0.51	0.06*	-0.38	-0.10	0.68*	0.62*	0.45*	-0.17	-0.39	-0.25	33.40
3	Coastal and interior plains (coastal dominant)	-1.00	-1.00	-0.95	-0.50	0.16	-0.81	-1.00	-0.14	2.54	1.78	3.71*	0.55
6	Tablelands	-0.55	-0.93	-0.77	0.40*	-0.15	-0.71	0.68*	-0.10	5.43*	4.86*	4.54*	2.32
8	Coastal and interior plains (interior dominant)	-1.00	-0.99	-0.90	0.07*	-0.49	-0.66	-0.74	0.19*	7.81*	10.33*	9.44*	4.42
5	High wet plains	-1.00	-1.00	-1.00	-1.00	-0.98	-1.00	-1.00	-0.80	7.77*	5.44	22.81*	0.31
	%area	0.86	6.43	6.68	1.93	58.71	8.55	2.99	8.71	0.73	0.82	3.59	100.00

Appendix B. Cross-classification table showing the comparison between our landform map and the soil map of Gabon by Martin (1981). CSB: Coastal Sedimentary Basin, NMS: Ngounie Nyanga Syncline, LKMM: Lambarene, Koumouna and Mayumbe massif, CMNM: Crystal Mountains and Ndjole Moutains, CM: Chaillu Mountains, FB: Francevilliens Basin, HHB: High Hills of Batéké, NP: North Plateaus. * = significant p-value for positive corrected frequencies of Chi-square by cell test

Present study		**Soil mapping units in Gabon, Martin et al. (1981)**								
Class	**Landform units**	**CSB**	**NNS**	**LKMM**	**CMNM**	**CM**	**FB**	**HHB**	**NP**	**% area**
9	Water	4.35*	-0.95	-0.87	-1.00	-1.00	-1.00	-1.00	-1.00	1.23
1	Low wet plains	4.35	-1.00	-0.75	-1.00	-1.00	-1.00	-1.00	-1.00	0.10
5	High Wet plains	2.85*	1.23*	-0.65	-0.98	-1.00	-0.97	-0.99	-0.78	1.71
3	Coastal interior plains (coastal dominant)	2.33*	0.61*	-0.39	-0.87	-0.88	-0.26	-0.98	-0.72	16.78
8	Coastal interior plains (interior dominant)	-0.20	3.83*	-0.47	-0.89	-0.76	-0.04	-0.65	-0.32	5.02
11	High mountain ranges	-0.93	-0.44	2.21*	3.80*	1.90*	-0.85	-1.00	-0.95	2.54
2	Foothills	-0.10	-0.13	0.48*	0.35*	0.42*	0.45*	-0.88	-0.41	22.99
12	Low-medium mountain ranges	-0.93	-0.26	1.24*	1.70*	1.75*	-0.15	-0.36	-0.80	16.44
7	High hills and crests	-0.82	0.00*	-0.33	-0.05	-0.24	1.00*	2.97*	-0.18	8.51
6	Tablelands	-0.78	-0.68	-0.97	-1.00	-0.92	-0.50	17.73*	-0.65	1.33
10	Low hills and plateaus	-0.88	-0.91	-0.93	-0.92	-0.76	-0.27	-0.81	2.00*	19.28
4	Dissected tablelands	-0.96	-0.88	-0.95	-0.96	-0.89	-0.19	4.47*	1.31*	4.07
	% area	18.48	9.28	4.67	5.22	17.23	14.04	4.00	27.08	100.00

Appendix C. Cross-classification table showing the comparison between our landform map and the probability map of vegetation types of the "Cuvette Centrale" wetlands by Dargie et al. (2017).

Present study		**Probability map of vegetation types in "Cuvette Centrale", Dargie et al. (2017)**					
Class	**Landform units**	**Water**	**Hardwood swamp**	**Savanna**	**Palm swamp**	**Terra firme forest**	**% area**
9	Water	143.51*	-0.22	2.27	-0.61	-0.95	0.41
1	Low wet plains	0.35*	6.58*	0.32	1.04*	-0.97	4.13
5	High wet plains	-0.32	2.25*	1.10*	1.31*	-0.63	14.82
8	Coastal interior plains (interior dominant)	-0.67	-0.33	0.43*	0.51	-0.11	24.27
3	Coastal interior plains (coastal dominant)	-0.94	-0.70	-0.11	-0.03	0.09*	10.63
6	Tablelands	0.16*	-0.98	-0.30	-0.91	0.35*	10.54
4	Dissected tablelands	-0.81	-0.97	-0.52	-0.65	0.30*	13.63
10	Low hills and plateaus	-0.98	-0.99	-0.78	-0.66	0.32*	13.78
7	High hills and crests	-0.87	-1.00	-0.84	-0.99	0.41*	4.92
2	Foothills	-0.95	-1.00	-0.92	-0.99	0.42*	2.69
12	Low-medium mountain ranges	-1.00	-1.00	-0.97	-1.00	0.42	0.17
	% area	0.49	7.34	3.76	18.08	70.28	100.00

Appendix D. Cross-classification table showing the comparison between our landform map and the 18-classes topographic map of Africa by Iwahashi & Pike (2007). * = significant p-value for positive corrected frequencies of Chi-square by cell test

Present Study		**18-classes topographic map in Africa, Iwahashi and Pike (2007)**																		
Class	**Landform units**	**18**	**17**	**16**	**14**	**12**	**10**	**15**	**13**	**8**	**11**	**6**	**9**	**7**	**5**	**4**	**2**	**1**	**3**	**% area**
9	Water	12.0*	3.1*	-1.0	-1.0	-1.0	-1.0	-0.9	-1.0	-1.0	-1.0	-1.0	-1.0	-1.0	-1.0	-1.0	-1.0	-1.0	-1.0	6.2
1	Low wet plains	-0.8	12.5*	34.2*	21.5*	0.4	-0.4	-0.7	-0.7	-1.0	-1.0	-1.0	-1.0	-1.0	-1.0	-1.0	-1.0	-1.0	-1.0	1.4
5	High wet plains	-0.3	5.1*	6.1*	8.5*	7.2*	7.2*	2.5*	1.8*	0.9*	-0.1	0.5*	-0.5	-0.9	-0.9	-0.9	-0.9	-1.0	-1.0	6.1
3	Coastal interior plains (coastal dominant)	-0.5	-0.1	-0.7	-0.5	-0.2	0.1*	1.9*	1.8*	-0.3	0.6*	-0.8	0.5*	-0.5	-0.7	-0.8	-0.9	-1.0	-0.9	7.2
8	Coastal interior plains (interior dominant)	-0.5	-0.5	-0.7	-0.7	1.5*	0.8*	1.1*	0.4*	2.5*	1.2*	1.2*	0.3*	0.0	-0.4	-0.3	-0.8	-0.9	-0.9	15.7
10	Low hills and plateaus	-0.9	-1.0	-1.0	-1.0	-1.0	-1.0	-0.2	0.4	-1.0	0.2*	-0.9	0.8*	-0.1	0.0	-1.0	-1.0	-0.9	-0.9	10.4
4	Dissected tablelands	-0.9	-1.0	-1.0	-1.0	-1.0	-1.0	-0.4	-0.2	-0.8	0.1*	-0.9	0.3*	0.3*	0.4*	-0.9	-0.9	-0.7	-0.8	15.9
2	Foothills	-0.8	-0.7	-1.0	-1.0	-1.0	-1.0	-0.7	-0.5	-0.8	-0.2	-0.9	-0.1	0.9*	0.4*	0.2*	-0.6	-0.1	0.5*	4.6
6	Tablelands	-0.9	-0.9	-1.0	-0.9	-0.9	-0.4	-0.8	-0.5	0.0	-0.4	1.4*	-0.1	0.2*	0.8*	-0.3	0.5*	0.1*	-0.5	20.4
7	High hills and crests	-0.9	-1.0	-1.0	-1.0	-1.0	-1.0	-0.9	-0.9	-0.7	-0.7	-0.7	-0.8	0.7*	0.3*	4.0*	3.1*	3.4*	2.8*	6.9
12	Low-medium mountain ranges	-0.9	-0.9	-1.0	-1.0	-1.0	-1.0	-0.9	-1.0	-0.9	-0.8	-0.9	-0.9	0.2*	-0.3	3.9*	4.6*	5.2*	7.1*	3.8
11	High mountain ranges	-1.0	-0.9	-1.0	-1.0	-1.0	-1.0	-1.0	-1.0	-0.9	-1.0	-1.0	-1.0	-0.7	-0.9	7.3*	8.4*	7.7*	10.9*	1.5
	% area	7.6	0.2	1.4	1.8	0.2	0.3	4.2	9.8	0.1	6.9	0.2	20.0	11.0	27.3	0.1	0.2	4.5	4.2	100.0

Appendix E. Specific PCA analyses on r-spectra used in FOTO: Correlation circles and illustration using arbitrary windows of texture gradients along axes 1 and 2 for windows of 1 km **(A)** and 10 km **(B)**.

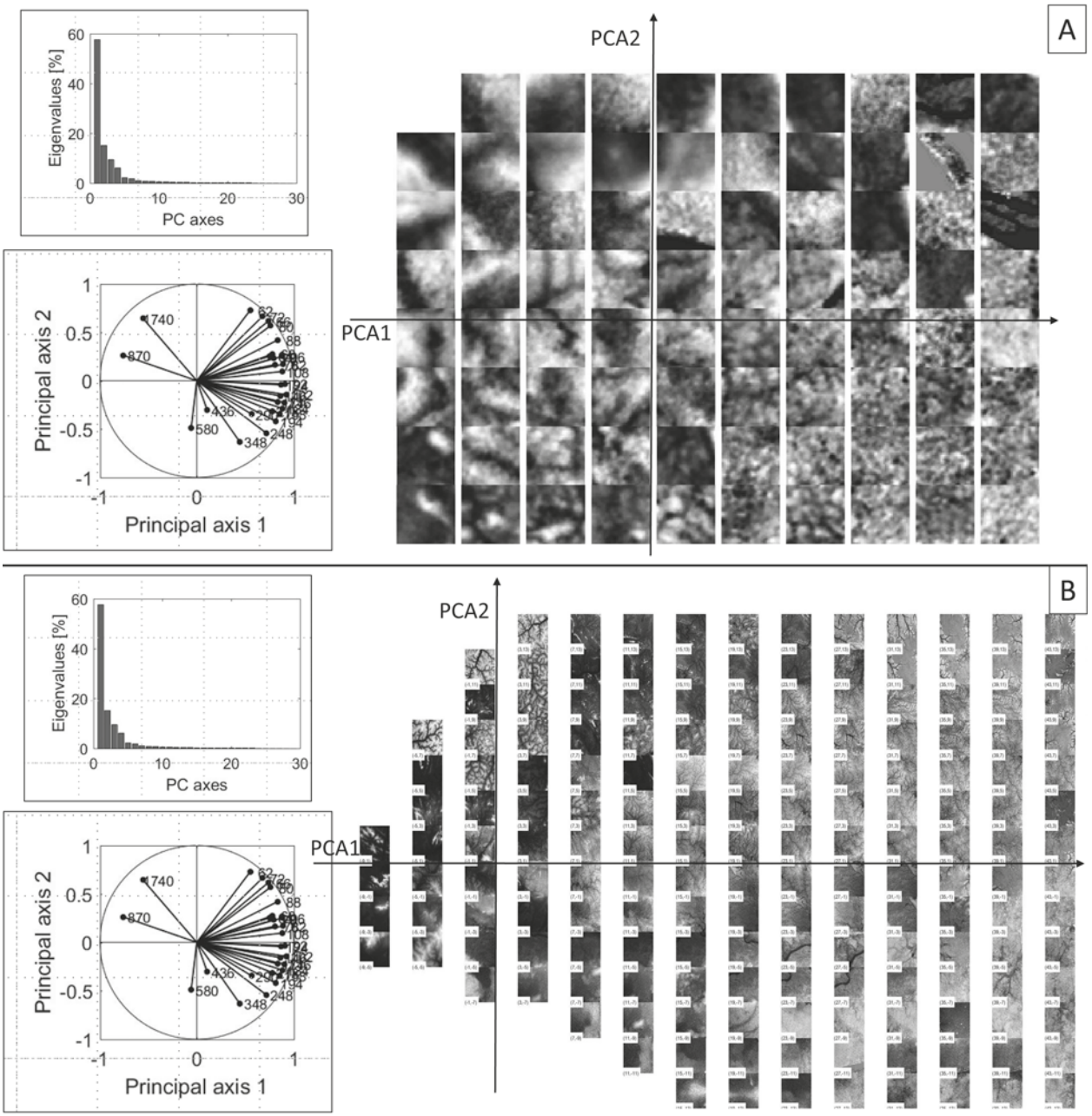

Appendix F. Histogram of tree cover (in percent, per pixel) for each class of our landform map.

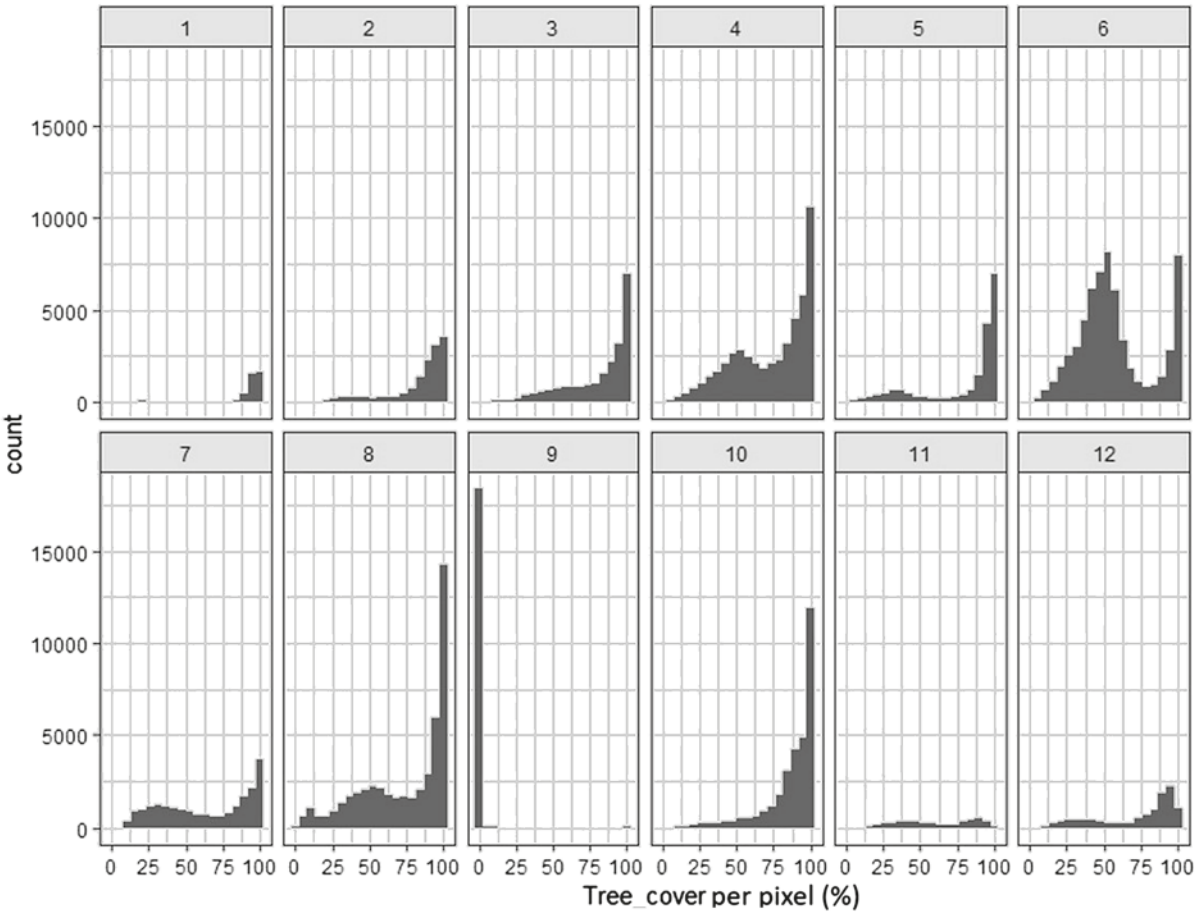

1- Low wet plains

2- Foothills

3- Coastal and interior plains (coastal dominant)

4- Dissected tablelands and mesas

5- High wet plains

6- Tablelands

7- High hills and crests

8- Coastal and interior plains (interior dominant)

9- Water

10- Low hills and plateaus

11- High mountain ranges

12- Low-medium montain ranges